



HAL
open science

Tandem metalloenzymes gate plant cell entry by pathogenic fungi

Bastien Bissaro, Sayo Kodama, Takumi Nishiuchi, Anna Maria Díaz-Rovira, Hayat Hage, David Ribeaucourt, Mireille Haon, Sacha Grisel, A. Jalila Simaan, Fred Beisson, et al.

► **To cite this version:**

Bastien Bissaro, Sayo Kodama, Takumi Nishiuchi, Anna Maria Díaz-Rovira, Hayat Hage, et al.. Tandem metalloenzymes gate plant cell entry by pathogenic fungi. *Science Advances*, 2022, 8 (51), 10.1126/sciadv.ade9982. hal-03918339

HAL Id: hal-03918339

<https://hal.inrae.fr/hal-03918339v1>

Submitted on 2 Jan 2023

HAL is a multi-disciplinary open access archive for the deposit and dissemination of scientific research documents, whether they are published or not. The documents may come from teaching and research institutions in France or abroad, or from public or private research centers.

L'archive ouverte pluridisciplinaire **HAL**, est destinée au dépôt et à la diffusion de documents scientifiques de niveau recherche, publiés ou non, émanant des établissements d'enseignement et de recherche français ou étrangers, des laboratoires publics ou privés.



Distributed under a Creative Commons Attribution 4.0 International License

Tandem metalloenzymes gate plant cell entry by pathogenic fungi

Bastien Bissaro^{1†}, Sayo Kodama^{2†}, Takumi Nishiuchi³, Anna Maria Díaz-Rovira⁴, Hayat Hage¹, David Ribeaucourt^{1,6,7}, Mireille Haon¹, Sacha Grisel¹, A. Jalila Simaan⁶, Fred Beisson⁸, Stephanie M. Forget⁹, Harry Brumer⁹, Marie-Noëlle Rosso¹, Victor Guallar^{4,5}, Richard O'Connell¹⁰, Mickaël Lafond⁶, Yasuyuki Kubo^{2*} and Jean-Guy Berrin^{1*}

¹INRAE, Aix Marseille Université, UMR1163 Biodiversité et Biotechnologie Fongiques, 13009, Marseille, France

²Faculty of Agriculture, Setsunan University, 573-0101, Osaka, Japan

³Division of Functional Genomics, Advanced Science Research Center, Kanazawa University, 920-0934 Kanazawa, Japan

⁴Barcelona Supercomputing Center, Plaça Eusebi Güell, 1-3, E-08034 Barcelona, Spain

⁵ICREA, Passeig Lluís Companys 23, E-08010 Barcelona, Spain

⁶Aix Marseille Université, CNRS, Centrale Marseille, iSm2, Marseille, France

⁷V. Mane Fils, 620 route de Grasse, 06620 Le Bar sur Loup, France

⁸CEA, CNRS, Aix Marseille Université, Institut de Biosciences et Biotechnologies d'Aix-Marseille (UMR7265), CEA Cadarache, 13108 Saint-Paul-lez-Durance, France

⁹Michael Smith Laboratories, University of British Columbia, 2185 East Mall, Vancouver, BC, V6T 1Z4, Canada

¹⁰INRAE, UMR BIOGER, AgroParisTech, Université Paris-Saclay, Thiverval-Grignon, France

*Correspondence to: Yasuyuki Kubo (yasuyuki.kubo@setsunan.ac.jp) and Jean-Guy Berrin (jean-guy.berrin@inrae.fr)

†These authors contributed equally

Abstract

Global food security is endangered by fungal phytopathogens causing devastating crop production losses. Many of these pathogens use specialized appressoria cells to puncture plant cuticles. Here, we unveil a pair of alcohol oxidase-peroxidase enzymes to be essential for pathogenicity. Using *Colletotrichum orbiculare*, we show that the enzyme pair is co-secreted by the fungus early during plant penetration, and that single and double mutants have impaired penetration ability. Molecular modeling, biochemical and biophysical approaches revealed a fine-tuned interplay between these metalloenzymes, which oxidize plant cuticular long-chain alcohols into aldehydes. We show that the enzyme pair is involved in transcriptional regulation of genes necessary for host penetration. The identification of these infection-specific metalloenzymes opens new avenues on the role of wax-derived compounds and the design of oxidase-specific inhibitors for crop protection.

Short title:

Fungal metalloenzymes drive plant invasion.

One Sentence Summary:

Fungal phytopathogens secrete tandem metalloenzymes that catalyze cuticle oxidation and drive plant cell entry.

44 Introduction

45 Fungal phytopathogens represent a serious threat to plant health (1) and global food
46 security (2). *Colletotrichum* and *Magnaporthe* species rank among the top 10 most devastating
47 fungal phytopathogens in the world and reduce crop yield by up to 30% (3). Despite being
48 separated by ca. 300 million years of evolution (4, 5), these fungi share remarkable similarities
49 in their infection strategy, notably the formation of a specialized cell dedicated to host
50 penetration called an appressorium (6–8) (**Fig. 1A**). This dome-shaped, darkly melanized cell
51 generates a high internal turgor and directs this mechanical pressure onto a needle-like
52 penetration peg (9–11), which emerges from a 2-500 nm pore at the appressorial base to
53 puncture the plant’s outer defensive barriers, namely the cuticle and epidermal cell wall.
54 Despite major advances in our understanding of the cellular processes preceding (6, 7, 11–14)
55 and following (15, 16) plant cell entry, the (bio)chemical reactions occurring at this nanoscale
56 plant-fungus interface and their role in host penetration are not fully elucidated.

57 Copper radical oxidases (CROs) are enzymes with diverse substrate specificities, and
58 have been extensively studied since the late 1960s (17). Today, CROs include galactose 6-
59 oxidases (GalOx) (17), glyoxal oxidases (18), and broad specificity primary alcohol oxidases
60 (AlcOx) (19, 20). Despite the detailed knowledge available on the enzymology and structure
61 of CROs, their biological function remains largely unknown. It has only been proposed that
62 glyoxal oxidases play a role in lignin degradation by fungal saprotrophs (18). During the course
63 of our previous work (19), we noted that genes encoding secreted AlcOx orthologs are
64 particularly widespread among phytopathogenic ascomycete fungi and are absent in plants.
65 Given that long-chain primary alcohols are components of the waxy cuticle of aerial plant
66 surfaces (21), we hypothesized that AlcOx could play a role in fungal pathogenesis.

67 In this study, we used a combination of ‘omics analyses to unveil the pairing of AlcOx
68 with a redox partner, namely heme-peroxidase, in some fungal plant pathogens of high
69 agricultural importance. We used wet enzymology and molecular modeling to demonstrate and
70 characterize the interplay between these metalloenzymes. Reverse genetics, live-cell imaging
71 and fungal transcriptomics allowed us to probe the *in vivo* function of the enzyme pair,
72 providing new molecular insights into the host penetration cascade.

73 Results

74 Discovery of the tandem Perox-AlcOx

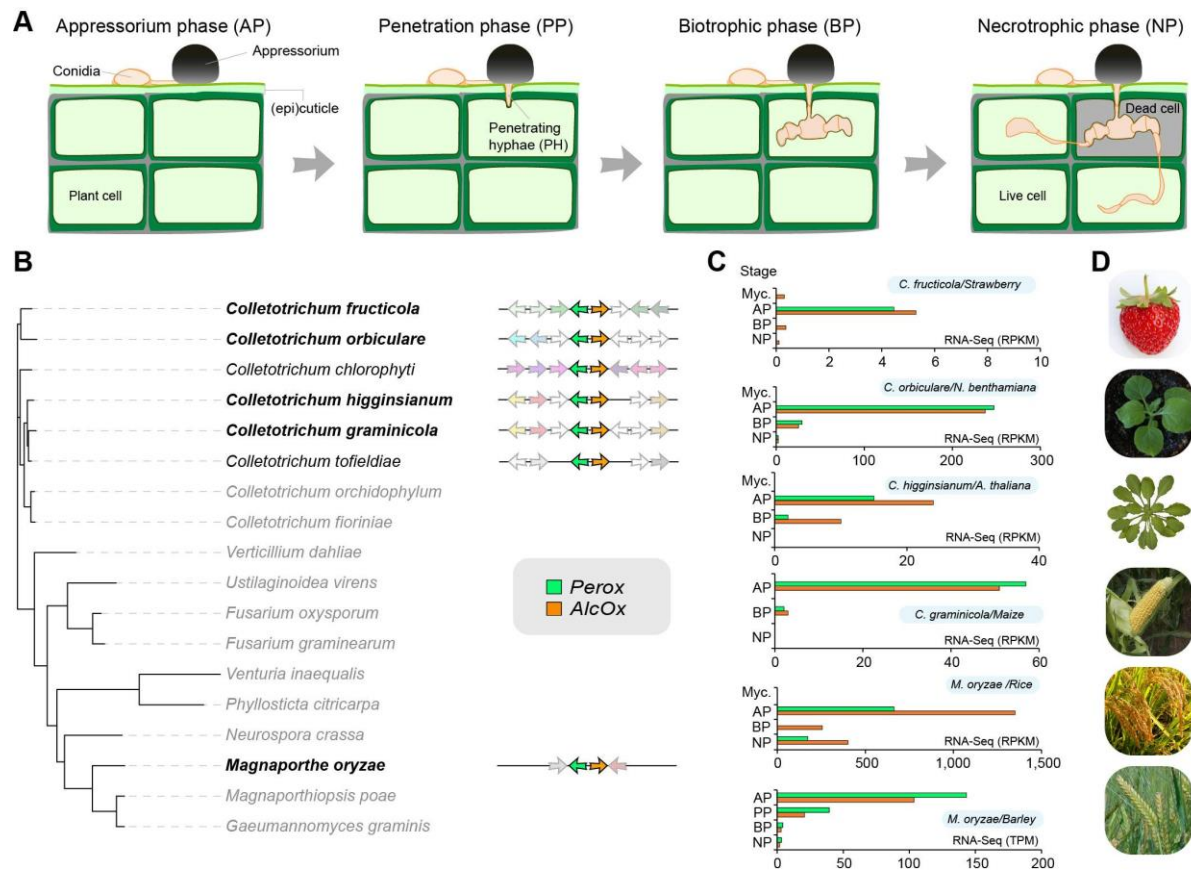
75 While studying the enzymology of *Colletotrichum* AlcOx enzymes for
76 biotechnological applications (19, 22), we noticed the presence of a gene encoding a putative
77 peroxidase located adjacent to an AlcOx-encoding gene (**Fig. 1B**). To strengthen this initial
78 observation, we searched for *alcox* orthologs in 30 sequenced *Colletotrichum* genomes, which
79 revealed the near-ubiquitous presence of a putative peroxidase (hereafter called “Tandem
80 Peroxidase”). Interestingly, the *perox* and *alcox* genes were found in a head-to-head
81 arrangement (**fig. S1**), suggesting the presence of a bidirectional promoter for tight co-
82 expression of the genes. Interestingly, these Tandem Peroxidases are never found in
83 combination with other types of CROs (**fig. S1C**) and both proteins encoded by the *perox-alcox*
84 pair are predicted to be secreted (**Table S1**). These observations aroused our interest because
85

86 it is known that CROs require activation by horseradish peroxidase (HRP) for maximum
87 activity *in vitro* (23, 24).

88 Our phylogenetic analysis of the peroxidase-catalase superfamily showed that the
89 Tandem Peroxidases cluster together in a sister clade within the under-explored ascomycete
90 Class II peroxidases (25) (**fig. S2A**). Furthermore, Tandem Peroxidases form a distinct clade
91 amongst the 333 Class II peroxidases found in *Colletotrichum* species (**fig. S2B**), suggestive
92 of neofunctionalization. A broad search for the co-occurrence of *perox* and *alcox* orthologs
93 across fungal genomes revealed that the pair is also present in *Magnaporthe* species, including
94 the infamous causal agent of rice blast, *Magnaporthe oryzae* (syn. *Pyricularia oryzae*) (**Table**
95 **S2**). Mapping the occurrence of Perox-AlcOx protein pairs and their corresponding genomic
96 neighborhoods onto a phylogeny of representative pathogenic ascomycetes (**Fig. 1B, fig. S3**)
97 allowed us to conclude that the pair is present in most *Colletotrichum* species complexes for
98 which genome sequences are available and in *Magnaporthe* spp., and that the head-to-head
99 organization of the pair is conserved in all these fungi, suggesting there is selection pressure to
100 retain the pairing and that it has a critical role in the biology of these pathogens (**Fig. 1B**).

101 To further test the hypothesis of a functional linkage of the *perox* and *alcox* gene
102 products, we parsed transcriptomic data available for those fungal species harboring the pair.
103 Remarkably, this analysis revealed that both genes are always tightly co-transcribed at the
104 appressorium stage in various pathosystems involving *Colletotrichum* species attacking maize,
105 fruits, and model plants (26, 27), and in *M. oryzae* attacking rice and barley (28, 29) (**Fig. 1C**
106 **and D**). In each case, the transcript levels are relatively low and detected within a narrow time
107 window, which may explain why these genes were overlooked in previous studies.

108



109
110
111
112
113
114
115
116
117
118
119
120
121
122

Fig. 1. Genomic and transcriptomic analysis of the Perox-AlcOx pair. (A) The multistage plant infection process of appressorium-forming fungi: appressorium (AP), penetration (PP), biotrophic (BP) and necrotrophic (NP) phases. (B) Phylogenomic occurrence of the *perox*-*alcOx* pair and consensus genomic environment (within each clade) amongst pathogenic ascomycetes (black bold lettering indicates species for which transcriptomics data are shown in panel C, and grey lettering indicates absence of the gene pair. Note that analogous tandem oxidases systems may occur in other fungi but were possibly not detected due to the stringent sequence identity thresholds used to define AlcOx and Perox-encoding genes. Selected *Colletotrichum* species and associated consensus sequences are representative of their respective species complexes; see **fig. S3**). (C) Time-course transcriptomic analysis of the Tandem Peroxidases (Perox, green) and AlcOx (orange) encoding genes (gene accession numbers in **Table S1**) during plant infection for different pathosystems (Myc., Mycelium) (26–29). Actual time points associated with each infection stages are provided in the Material and Methods section. (D) Illustration of targeted plant hosts.

123 Tandem Perox-AlcOx oxidize plant long chain alcohols

124 As a prelude to analyzing their biological function *in vivo*, we studied the substrate
125 specificity and enzyme interplay of the Perox-AlcOx pair *in vitro* (**Fig. 2A**). *C. orbiculare* was
126 selected as a model because it not only causes the economically important anthracnose disease
127 of cucurbits (e.g., melons, cucumber) but also has been used for decades as a model system for
128 studying fungal pathogenesis (30). Despite the notorious difficulties associated with
129 heterologous expression of such metalloenzymes, we successfully produced in the yeast *Pichia*
130 *pastoris* recombinant copper-radical AlcOx and heme-iron tandem peroxidase from *C.*
131 *orbiculare* (hereafter *CorAlcOx* and *CorPerox*, respectively). Similar to the previously studied
132 AlcOx orthologs from *C. graminicola* and *C. gloeosporioides* (19) (**fig. S1A**), *CorAlcOx*
133 oxidized both aromatic and long-chain aliphatic primary alcohols (**fig. S4A**). This finding
134 raises the possibility that fatty primary alcohols present in the cuticle of many plant species
135 (21), including cucumber, could be the native substrates of these enzymes.

136 On the other hand, *CorPerox* was confirmed to be a peroxidase, albeit with moderate
137 catalytic efficiency ($k_{\text{cat}} = 1.52 \pm 0.02 \text{ s}^{-1}$, $K_{\text{M}}^{\text{H}_2\text{O}_2} = 80 \pm 3 \text{ }\mu\text{M}$, $k_{\text{cat}}/K_{\text{M}} = 1.9 \times 10^4 \pm 0.1 \text{ s}^{-1} \text{ M}^{-1}$)
138 compared to the only previously characterized ascomycete Class II peroxidase (25),
139 commercial horseradish peroxidase (HRP) (31), and well-studied basidiomycete lignin-active
140 peroxidases (32) ($k_{\text{cat}}/K_{\text{M}} = 10^4\text{-}10^7 \text{ s}^{-1} \text{ M}^{-1}$). *CorPerox* was only active on low redox-potential
141 substrates and not on any of the substrates of canonical lignin-active peroxidases (**fig. S4B**),
142 and required the presence of calcium ions for stability (**fig. S4C**). These observations are in
143 agreement with structural predictions (**fig. S5**), which indicate the presence of two conserved
144 calcium ion binding sites, but absence of the manganese binding site and the surface-exposed
145 tryptophan involved in long-range electron transfer, which are two key features of lignin-active
146 peroxidases (33).

147 Despite its comparatively low peroxidase activity, *CorPerox* activates *CorAlcOx* for
148 oxidation of primary alcohols in a dose-dependent manner, and to a much greater extent than
149 the plant peroxidase HRP does (**Fig. 2B**). The pH optima of *CorAlcOx* and *CorPerox* were
150 markedly different (ca. 8 and 4, respectively, **fig. S4D**). Importantly, the pH of the environment
151 measured on cucumber cotyledons at the time of triggering appressorium penetration by *C.*
152 *orbiculare* was between 7.5 and 8.0. Taken together, these results indicate that AlcOx
153 activation is not dependent on highly efficient peroxidase activity. We also heterologously
154 produced the Perox-AlcOx pair from the rice blast pathogen *M. oryzae*, of which *MorAlcOx*
155 was recently confirmed to be a primary alcohol oxidase (34). Here, we obtained an activation
156 profile for the *MorPerox-MorAlcOx* pair resembling that observed for the *C. orbiculare* pair
157 (**fig. S4E cf. Fig. 2B**).

158 Having determined optimal enzyme activation conditions, we then probed further the
159 activity of the *CorPerox-CorAlcOx* pair on biologically relevant aliphatic alcohols. Despite
160 challenges associated with substrate solubility in aqueous buffer, we clearly detected activity
161 on hexadecan-1,16-diol and octadecan-1-ol, as well as on a crude preparation of waxes
162 extracted from cucumber cotyledons (**Fig. 2C**). Importantly, such activity was detected only
163 when both enzymes were present. Product analysis by gas chromatography unambiguously
164 indicated that octadecan-1-ol was oxidized to the corresponding aldehyde (**fig. S4F**).

165 To obtain a deeper understanding of the activation of AlcOx by the Tandem Peroxidase,
166 we analyzed electron transfer by electron paramagnetic resonance (EPR) spectroscopy (**Fig.**

167 **2D**) and state-of-the art molecular modeling (**Fig. 2E and fig. S6**). Reduction in the EPR signal
168 of the *inactive* Cu(II)-non-radical form of *CorAlcOx* upon addition of *CorPerox* was
169 supportive of one-electron oxidation leading to the EPR silent, *active* Cu(II)-radical form (**Fig.**
170 **2A and D**). This change in electronic structure, observed in the absence of any substrate,
171 confirms the activity-independent activating role of *CorPerox*. It also indicates a close contact
172 between the enzymes during the activation process, which is concordant with our modeling
173 studies (see below) and with the sigmoidal, titration-like curves observed during activity assays
174 carried out in the presence of substrate (**Fig. 2B**). Further, *CorAlcOx-CorPerox* top 5 models
175 predicted by two independent computational techniques, PIPER (35) and AlphaFold2-
176 Multimer (36) consistently placed *CorPerox* structures in front of the *CorAlcOx* active site
177 (**fig. S6A**). Refinement of these models with the all atom Monte Carlo software PELE (37),
178 which includes protein small rotations and translations followed by an exhaustive side-chain
179 prediction at the interface, resulted in a clear minimum (**fig. S6B**) where the heme group of
180 *CorPerox* is oriented towards the *CorAlcOx* copper ion (**Fig. 2E and fig. S6C**). Notably, the
181 binding surfaces of AlcOx orthologs are considerably more hydrophobic than that of GalOx
182 (**fig. S7A and B**), which is consistent with the idea that AlcOx may have evolved to interact
183 with the hydrophobic plant cuticle. Moreover, in the top model (**Fig. 2E**), there is a significant
184 decrease of solvent exposure of the *CorAlcOx* active site, defining a cavity between both
185 enzymes that could facilitate diffusion and binding of a long-chain alcohol substrate. C18
186 docking and PELE induced fit simulations confirm this point, revealing a pronounced local
187 minimum in which the alcoholic group of the substrate is well-positioned for catalysis (**fig.**
188 **S6D**).

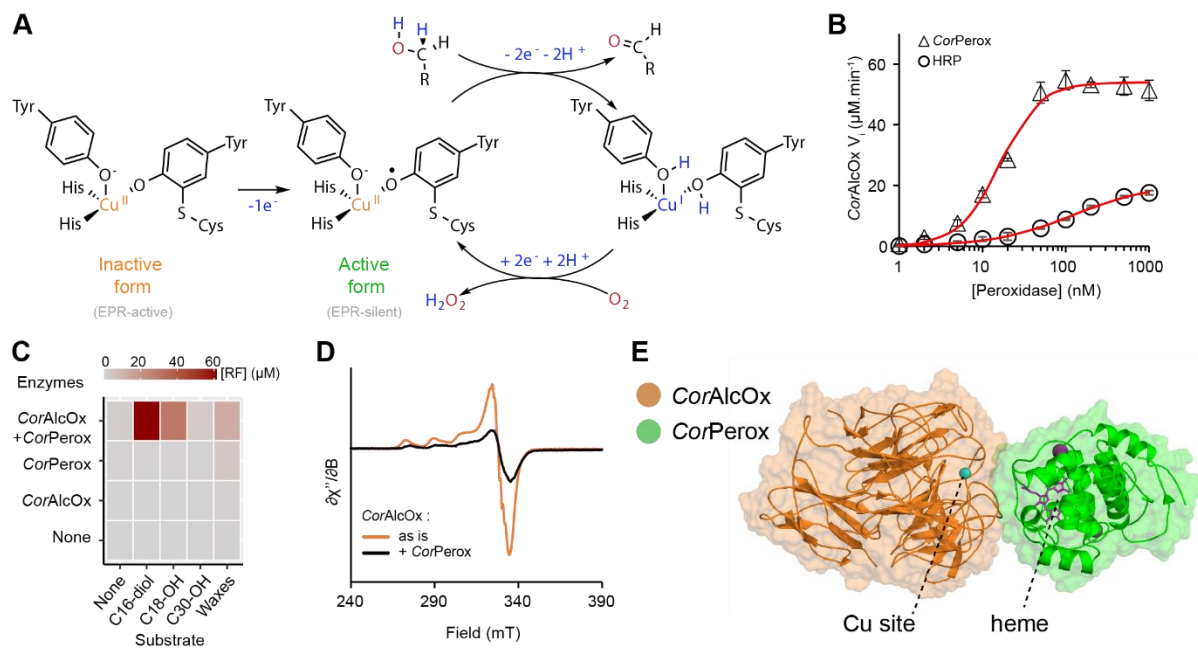
190
191

Fig. 2. Biochemical and biophysical evidence for interplay between *CorPerox* and *CorAlcOx*.

192 Reaction mechanism of CROs showing activation of the resting, inactive form of the enzyme via
 193 formation of a tyrosine radical, yielding the Cu(II)-radical active form. The latter will oxidize an alcohol
 194 into the corresponding aldehyde followed by regeneration of the active form via the two-electron
 195 reduction of O_2 into H_2O_2 . (B) *CorAlcOx* oxidation rate of benzyl alcohol in presence of varying
 196 amounts of HRP or *CorPerox*. (C) Activity of *CorPerox-CorAlcOx* on crude extract of cucumber waxes
 197 and derived long-chain aliphatic alcohols, monitored via the production of chromogenic resorufin (RF),
 198 product of the Perox-catalyzed oxidation of Amplex-Red by H_2O_2 , the latter being the co-product of
 199 AlcOx-catalyzed oxidation of primary alcohols into aldehydes. (D) EPR spectra of inactive *CorAlcOx*
 200 before (orange curve) and after mixture with *CorPerox* (black curve). EPR parameters of the Cu(II)
 201 inactive form: $g_z = 2.270$, $A_z^{\text{Cu}} = 171 \cdot 10^{-4} \text{ cm}^{-1}$, $g_x = 2.047$, $A_x^{\text{Cu}} < 50 \cdot 10^{-4} \text{ cm}^{-1}$, $g_y = 2.054$,
 202 $A_y^{\text{Cu}} < 50 \cdot 10^{-4} \text{ cm}^{-1}$ and super-hyperfine coupling constant corresponding to two N-ligands $A^{\text{N}} = 43 \cdot 10^{-4} \text{ cm}^{-1}$. (E)
 203 Lowest energy *CorAlcOx-CorPerox* complex obtained by protein-protein modeling simulation with
 204 PELE (see **fig. S6** for more details). The copper atom is shown as a blue sphere, the heme group as
 205 magenta sticks and calcium ions as purple spheres.
 206

207 **The Perox-AlcOx pair gates plant penetration**

208 To investigate the role of the Perox-AlcOx pair in plant infection, we isolated single
209 and double gene deletion mutants of *C. orbiculare* (**fig. S8**). Inoculation of spore suspensions
210 onto intact cucumber cotyledons showed that fewer and smaller lesions were formed by all the
211 mutants compared to the wild-type strains (**Fig. 3A and B**). For instance, the proportion of
212 lesions with a diameter > 4 mm fell from 95 % to < 20%. Furthermore, similar phenotypes
213 were obtained for single and double mutants, suggesting that both oxidases are crucial for
214 fungal pathogenicity.

215 Further investigations indicated that neither single nor double *perox/alcox* deletion
216 mutants were affected in mycelial growth (**fig. S8A**). Microscopy revealed that the significant
217 loss of pathogenicity of the mutants was due to a large decrease in the frequency of host
218 penetration (**Fig. 3C**). However, morphogenesis, cell wall melanization, and turgor build-up
219 within appressoria cells were virtually indistinguishable from those of the wild-type strain (**fig.**
220 **S8B-D**). The next step in the infection process is the emergence of a needle-like penetration
221 peg through a pore in the basal cell wall of the appressorium (**Fig. 1A**), during which actin
222 assembly at the pore provides rigidity (38). Using a red fluorescent protein/actin-binding
223 protein fusion (Lifeact-RFP), we found normal actin assembly at the appressorium pore for
224 both the single and double mutants inoculated onto cucumber cotyledons (**fig. S8E and F**).

225 Remarkably, the mutants could penetrate and form hyphae inside inert cellophane
226 membranes (**fig. S9A-C**) and caused wild-type-like lesions when inoculated on mechanically
227 wounded cucumber cotyledons (**Fig. S9D and E**), in contrast to the crippled invasive capacity
228 observed on intact cotyledons (**Fig. 3C**). This points to a mechanism involving plant surface
229 compounds, concordant with the catalytic activity of the Perox-AlcOx pair (**Fig. 2C**). These
230 results collectively indicate that *CorAlcOx* and *CorPerox* play a crucial role during the early
231 penetration stage, but are not involved in either appressorium or peg formation.

232 To further examine the function of the Perox-AlcOx pair during plant infection, we
233 attempted to localize the proteins by live-cell imaging of *CorAlcOx*-mCherry and *CorPerox*-
234 GFP driven by their native promoters. Although the *CorAlcOx*-mCherry and *CorPerox*-GFP
235 complemented the defect in pathogenicity of the deletion mutants, fluorescence of *CorAlcOx*-
236 mCherry and *CorPerox*-GFP was not detectable during appressorium formation on cucumber
237 cotyledons (**fig. S10A**), suggesting that gene expression was too low, consistent with
238 transcriptomic data (**Fig. 1C**), or that the gene products were secreted and diffused away from
239 the penetration site. However, the constitutive overexpression of *CorAlcOx*-mCherry and
240 *CorPerox*-GFP, driven by the *translation elongation factor (TEF)* promoter, revealed that both
241 proteins accumulated specifically at the appressorial penetration pore and that signal intensity
242 increased during penetration peg formation (**Fig. 3D, fig. S10B and C, and Supplementary**
243 **Movie 1**). This protein co-localization observed *in vivo* is consistent with gene co-expression
244 data (**Fig. 1C**) and rationalizes the co-operative activity demonstrated by biochemical assays
245 (**Fig. 2**). Remarkably, *CorAlcOx*-mCherry and *CorPerox*-GFP were detected at the plant
246 surface beneath detached appressoria, at the penetration site (**Fig. 3E**), suggesting that the
247 tandem metalloenzymes are secreted from appressoria into the plant epidermis. Strikingly,
248 *CorAlcOx*-mCherry and *CorPerox*-GFP were not detected at the penetration site on cellophane
249 membranes (**fig. S10D**), suggesting that interaction of the fungus with the plant surface triggers
250 local and specific recruitment of the tandem metalloenzymes to the pore.

251

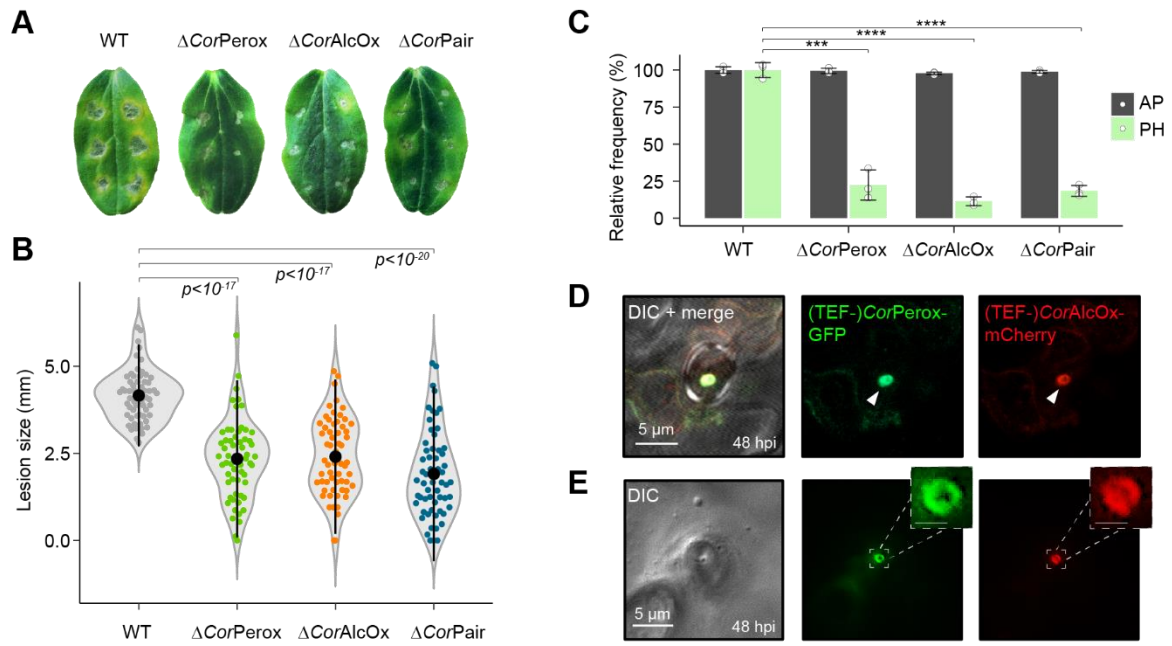
252 To probe the presence of potential natural substrates of the fungal AlcOx in the
253 neighborhood of the penetration site, we carried out a compositional analysis of waxes present
254 at the surface of uninoculated cucumber cotyledons (**fig. S11**). This analysis showed that the
255 extracted waxes are mainly composed of odd-numbered alkanes (C27-C33) and even-
256 numbered long-chain primary alcohols (C24-C32). Fatty aldehydes were found only as traces.
257 Thus, this experiment demonstrates that potential substrates of AlcOx represent a major part
258 of the plant cuticular compounds while AlcOx reaction products are very minor components.

259 To further explore the role of Perox-AlcOx in the fungus-plant dialogue, we exposed
260 the *C. orbiculare* single and double mutants to a product of the AlcOx, *viz.* the aliphatic long
261 chain aldehyde *n*-octadecanal. For all gene deletion mutants, the addition of *n*-octadecanal
262 partially restored appressorium penetration ability and lesion formation on cucumber leaves
263 (**Fig. 4A and B**), suggesting that the role of the fungal Perox-AlcOx pair is to generate long
264 chain aldehydes to prime the fungus for efficient plant infection.

265 Taken together, our results suggest that the role of the fungal Perox-AlcOx pair is to
266 increase locally the concentration of long-chain aldehydes. These aliphatic compounds,
267 members of the volatile organic compounds, are well-known to function as signal molecules
268 (39), raising the possibility that the Perox-AlcOx pair generates signals to prime the fungus for
269 efficient plant infection.

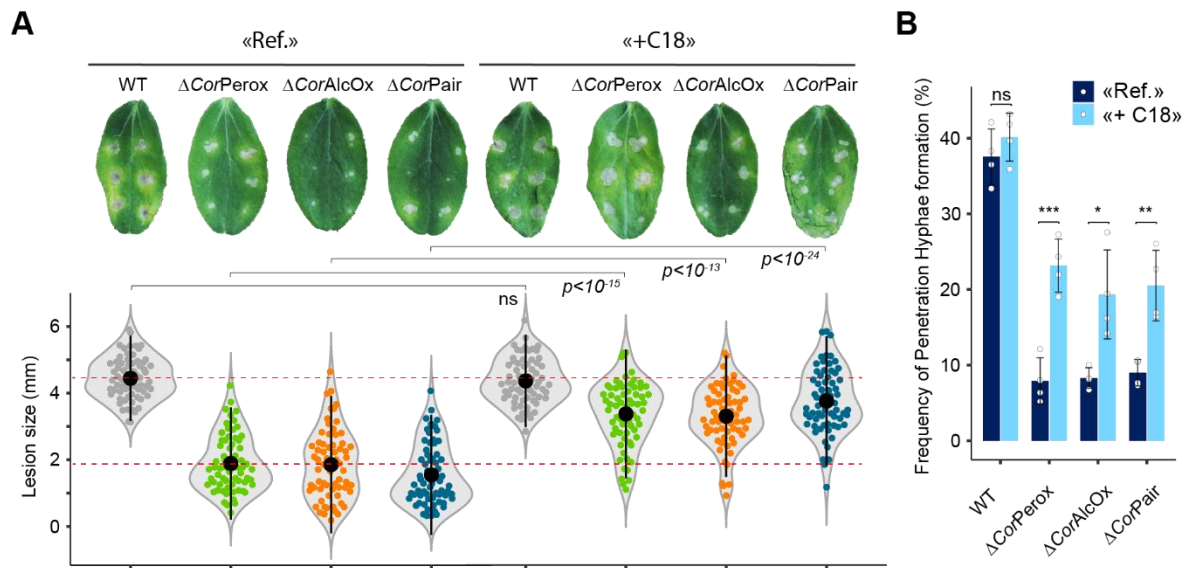
270

271 To gain insights into the possible steps controlled by the Perox/AlcOx activities during
272 the early infection process, we performed comparative transcriptomic analyses of *C. orbiculare*
273 wild-type and double mutant strains at the appressorial stage on cucumber leaves and
274 cellophane (**Fig. 5**). Analysis of the differentially-expressed genes suggested that the Perox-
275 AlcOx pair contributes to the regulation of a subset of 32 plant-inducible genes predicted to
276 encode small secreted proteins (SSPs), carbohydrate-active enzymes (CAZymes) and
277 membrane transporters (**Table S6**). SSPs and CAZymes are well-known fungal effectors
278 playing a key role in the molecular dialog with host plants. A phylogenetic analysis of
279 CAZymes (**Table S6**) present in this subset of genes revealed that the pair is required for the
280 up-regulation of genes encoding proteins directed towards the plant cell wall (PCW) and the
281 fungal cell wall (FCW) (**Fig. 5**). Among the former, we detected cellulose-active enzymes
282 known to display an enzymatic interplay – *viz.* the cello-oligosaccharide dehydrogenase AA7
283 and the lytic polysaccharide monooxygenase (LPMO) AA9 (40) – as well as pectin-active
284 enzymes from the PL1, PL3 and GH93 CAZy families. Regarding the FCW-targeting proteins,
285 we detected three proteins with carbohydrate binding modules (CBM50s; also called LysM
286 domains) that bind to chitin and function to evade recognition by host immune receptors during
287 infection (41).



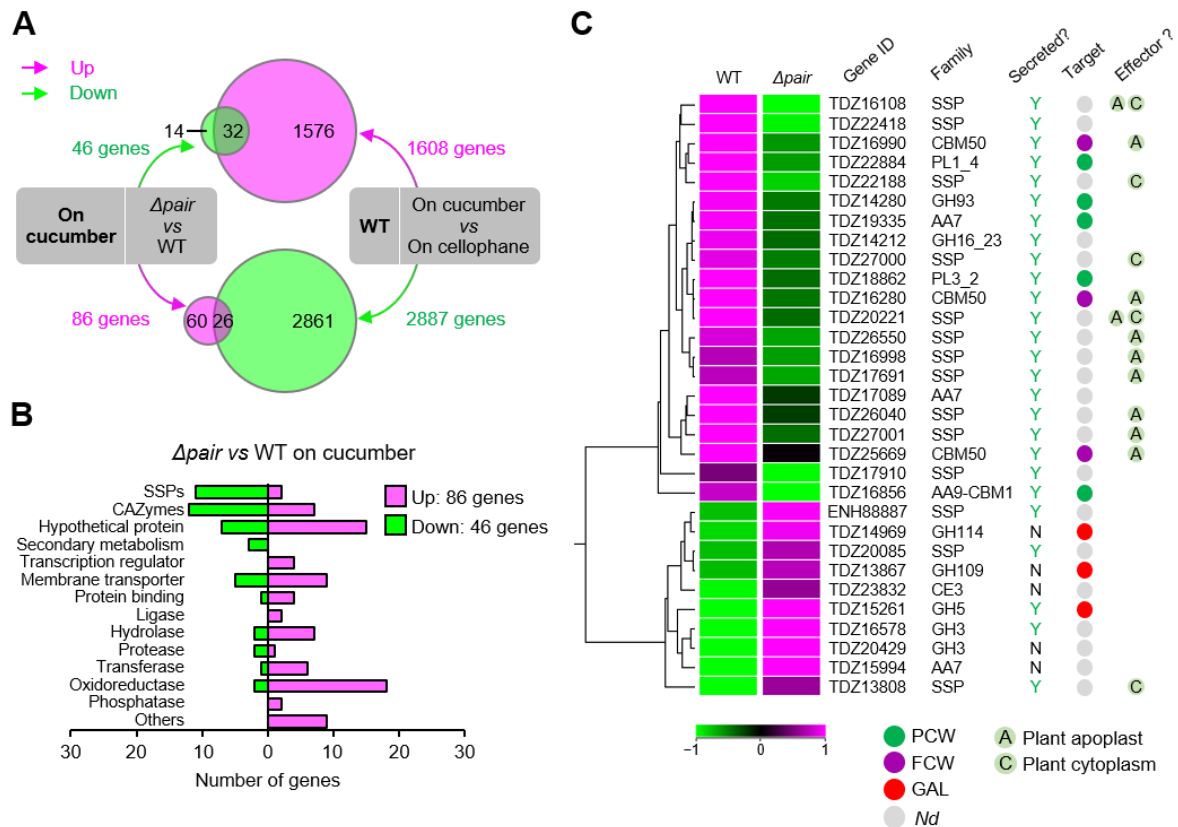
288
289
290
291
292
293
294
295
296
297
298
299
300
301
302

Fig. 3. *In vivo* characterization of the role of the Perox-AlcOx pair during plant infection. **A-B,** Infection phenotypes (**A**) and violin plot of the necrotic lesions size (**B**), at 5 dpi, for the wild-type (WT) and *perox/alcox* deletion mutants of *C. orbiculare* on intact cucumber (*Cucumis sativus*) cotyledons. For each strain/plant combination, at least 60 inoculations were carried out. (**C**) Relative frequency (WT set to 100%) of development of normal appressorium (AP) and penetrating hyphae (PH) by *C. orbiculare* strains on cucumber cotyledons. Data are presented as average values (>300 appressoria for each replicate, n = 3 independent biological replicates) and error bars show s.d.. (**D-E**) Localization of the *C. orbiculare* tandem oxidases on cotyledons at 48 hpi, in the presence of appressoria cells (**D**) or after detachment of the appressoria from the surface of the leaf (**E**). See **movie S1** for a 3D view. In panel **D**, white arrowheads indicate enzyme accumulation at the appressorium pore. In panel **E**, enlarged insets show a ring-like localization of the enzymes (scale bar = 1 μ m). In panels **B-C**, a one-tailed independent *t*-test for each mutant vs WT was applied (***) $P < 0.001$, ****) $P < 0.0001$).



303
 304
 305
 306
 307
 308
 309
 310
 311
 312
 313
 314

Fig. 4. Effect of *n*-octadecanal on the pathogenicity of *perox/alcox* deletion mutants. The figure shows the effect of the addition of 10 μM *n*-octadecanal (denoted as +C18) on necrotic lesions size formed by *C. orbiculare* WT and mutant strains on cucumber cotyledons (24°C, 5 days) (A) and on the formation of penetration hyphae (B). Control experiments, i.e. 1% ethanol without addition of *n*-octadecanal, are denoted as Ref. In panel A, for each strain, we show one representative cotyledon image of the infection phenotype and, below, a violin plot of lesions sizes based on 66 inoculation sites per condition (carried out over 4 independent biological replicates). In panel B, data are presented as mean percentages (>300 appressoria per replicate, n = 4 independent biological replicates) and error bars show s.d. In panels A and B, for each strain, a one-tailed independent *t*-test of +C18 vs Ref was applied.



315

316

317

318

319

320

321

322

323

324

325

326

327

328

329

330

331

332

333

334

335

336

337

Figure 5. Loss of the Perox-AlcOx pair affects fungal gene expression during appressorium-mediated penetration of *C. orbiculare*. (A) Venn diagrams illustrating the differentially regulated (up- or down-regulated) genes between cucumber vs cellophane that are under control of the AlcOx-Perox pair. **Top:** green circle indicates the number of downregulated genes (46 genes) in $\Delta pair$ compared with wild-type strain (WT), both incubated on cucumber; magenta circle denotes the number of genes (1608 genes) upregulated on cucumber vs cellophane in the WT strain. **Bottom:** Magenta circle indicates the number of upregulated genes (86 genes) in $\Delta pair$ compared with WT, both incubated on cucumber; green circle shows the number of downregulated genes (2887 genes) in the WT strain on cucumber vs cellophane. In the top and bottom Venn diagrams, the overlap indicates that 32 and 26 genes are respectively upregulated or downregulated in the presence of the plant and also under control of the AlcOx-Perox pair. (B) Class-wise distribution of the number of genes that were differentially expressed in appressoria of the $\Delta pair$ double mutant compared with WT on cucumber cotyledons. (C) Hierarchical clustering heatmap of differentially expressed genes encoding CAZymes and SSPs in the $\Delta pair$ mutant compared to WT on cucumber cotyledon. The expression values per gene were median normalized. The columns were clustered by Euclidean distance. The expression levels of up- (magenta) and down-regulated (green) genes are shown as log₂-transformed values. On the right-hand side of the figure, we show the presence of a predicted signal peptide (Y, Yes; N, No), phylogeny-based substrate specificity predictions for CAZymes (PCW, plant cell wall; FCW, fungal cell wall; GAL, galactose-containing compounds; Nd, not determined) and SSPs/CBM50s that are putative effectors (pale green circles) predicted to localize in the plant cell (in the apoplast (A) and/or the cytoplasm (C)). See **Table S6** for more details.

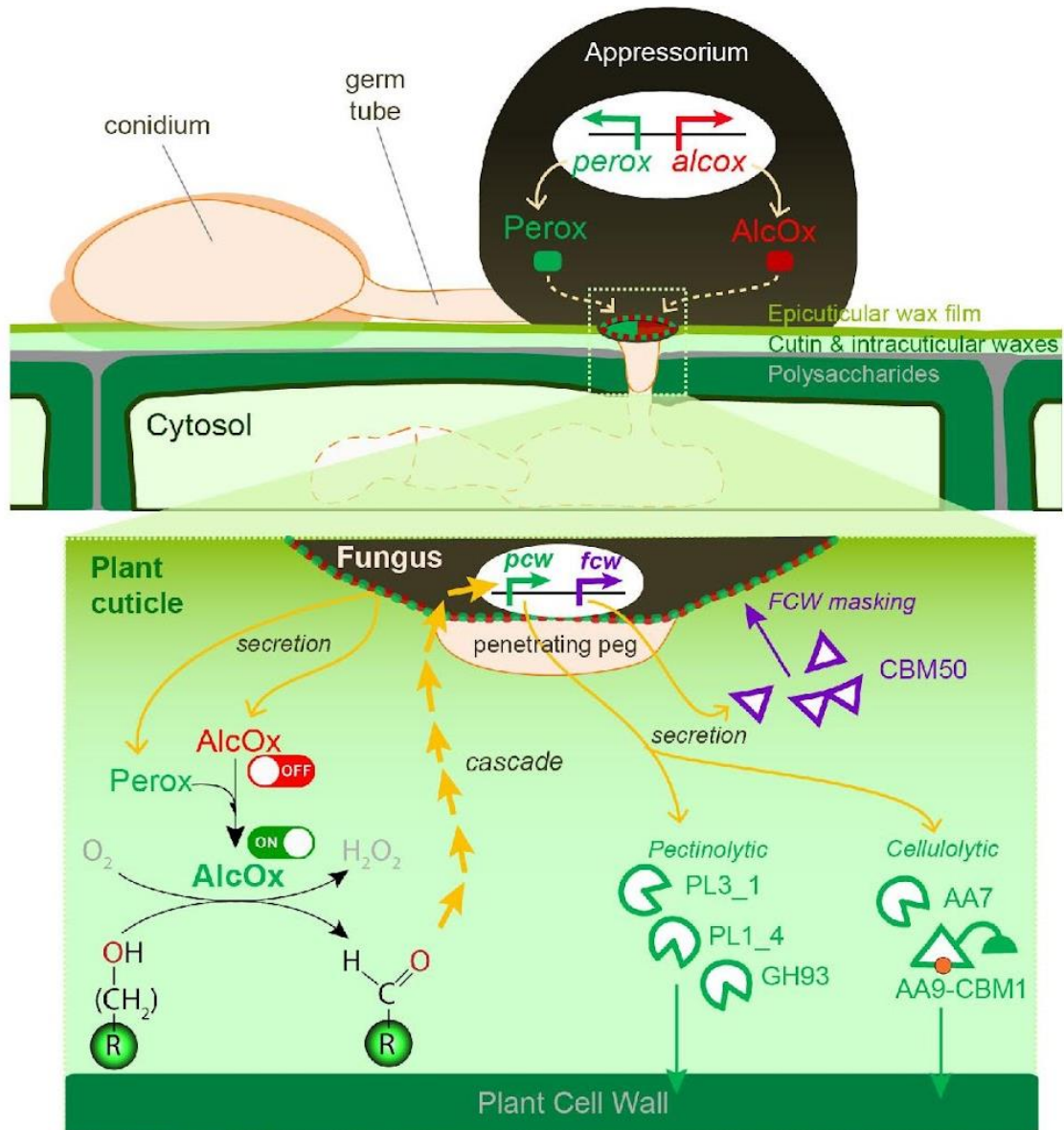
338 Discussion

339 Research on plant invasion by appressorium-forming fungi teaches us that the
340 development of these specialized infection structures is an extremely complex, finely regulated
341 process. In this study, we have shown that fungal AlcOx, which are only encountered in
342 phytopathogens, have a very different biological function than the few distantly-related CROs
343 for which roles in morphogenesis (42, 43) or lignin degradation (18) were proposed. We
344 showed that the tandem Perox-AlcOx metalloenzymes are specifically deployed at the
345 initiation of penetration peg formation and their localization at the pore formed at the fungus-
346 plant cell interface. Our results suggest that the oxidative action of Perox-AlcOx on long-chain
347 alcohols triggers a yet-to-be-elucidated biochemical cascade leading to penetration. Indeed,
348 functional complementation of the deletion mutants, which were defective in their ability to
349 puncture intact plant cuticles, by the product of the reaction suggests that cuticular alcohol
350 oxidation provides a chemical cue required for plant cell entry (Fig. 6). We speculate that
351 acquisition of the Perox-AlcOx pair provided the ecologically widespread *Colletotrichum* and
352 *Magnaporthe* species with an advantage, namely an *in-house* “locksmith” (i.e. the tandem
353 metalloenzymes) ensuring localized production of the aldehyde. This entry key is needed to
354 move to the next pathogenesis stage with the expression of PCW-degrading enzymes to
355 facilitate penetration, and of FCW-binding proteins and carbohydrate oxidases to evade host
356 immunity. For example, it has been suggested that, upon oxidation by fungal LPMOs and
357 oligosaccharide oxidases, plant oligosaccharides can no longer play their role as inducers of
358 host immune response (40, 44, 45).

359 It is interesting to speculate why Nature has evolved such a complex enzymatic system
360 relying on heme-iron peroxidase and elaborate copper radical chemistry when simpler, mono-
361 enzyme systems could be employed for the same purpose (e.g. FAD-dependent oxidases active
362 on long-chain alcohols (46)). We show that the functional integrity of the secreted tandem
363 metalloenzymes system endows pathogenic fungi with fine control over oxidation reactions in
364 the extracellular space. We propose that the copper-radical center equips CROs with a “redox
365 switch” to turn on activity with high spatio-temporal resolution, when paired with a cognate
366 peroxidase (Fig. 6). More generally, our study suggests that fungi have evolved ways of
367 controlling oxidative reactions that are seemingly out of reach, i.e. beyond the bounds of the
368 fungal plasma membrane and cell wall, through tight genetic regulation and protein interplay
369 between secreted oxidoreductases.

370 In conclusion, using a combination of *in silico*, *in vitro* and *in vivo* approaches, we have
371 unveiled the existence of a natural redox partner, i.e. a heme-peroxidase, for AlcOx-type CROs,
372 and showed that the pair acts as a secreted virulence factor during early infection (Fig. 6). It is
373 noteworthy that the enzymology-driven approach pursued here was essential to bring to light
374 this unique mechanism, because low expression levels, fine temporal tuning, and highly
375 localized co-secretion of the Perox-AlcOx would have evaded classical ‘omic approaches. The
376 specific occurrence of the Perox-AlcOx pair in most *Colletotrichum* and *Magnaporthe* species
377 raises the possibility that functionally equivalent, coupled oxidative enzymatic mechanisms
378 may operate in other appressorium-forming fungal pathogens. We anticipate that the present
379 discovery will open new research avenues, notably on the role of wax-derived compounds in
380 the cascade of events leading to successful infection as well as on the development of oxidase-
381 specific inhibitors as surface-acting, anti-penetrant drugs for crop protection.

382
383



384
385
386
387
388
389
390
391
392

Fig. 6. Schematic summary of the recruitment of the fungal Perox-AlcOx pair during early plant penetration and its proposed role in the induction of a biochemical cascade. The bottom panel is a zoom-in view illustrating the Perox-AlcOx reaction occurring at the fungus-plant interface and the triggered downstream cascade, highlighting the induction of genes encoding proteins targeting the plant cell wall (*pcw*) and fungal cell wall (*fcw*).

393 **Materials and Methods**

394

395 **Chemicals and commercial enzymes**

396 Most chemicals were purchased from Sigma (Darmstadt, Germany) or VWR (Fontenay-sous-
397 Bois, France) unless stated otherwise. Molar concentrations of type II HRP (Sigma-Aldrich;
398 MW 33.89 kDa) were estimated by Bradford assay. *n*-octadecanal was purchased from TCI-
399 Europe (Zwijndrecht, Belgium). All alcohol substrates stock solutions were prepared either in
400 H₂O or in acetone and stored at -20°C. The concentration of H₂O₂ stock solution was verified
401 at 240 nm ($\epsilon^{240} = 43.6 \text{ M}^{-1} \cdot \text{cm}^{-1}$).

402

403 **Bioinformatics**

404 Species tree of the 18 ascomycete genomes (shown in **Fig. 1b**) was constructed as previously
405 described (47). Core clusters containing only one protein-coding gene per species were
406 identified using FastOrtho (48) with the following parameters: 50% identity and 50% coverage.
407 Each cluster was aligned with MAFFT 7.221 (49), and curated alignments were concatenated
408 with Gblocks 0.91b (50). The tree was finally constructed with RAxML 7.7.2 (51)
409 (PROTGAMMAWAG model and 500 bootstrap). Phylogenetic analysis of AA5_2 genes and
410 «standard» haem peroxidases (PFAM 00141, including Class II peroxidases) from 30
411 *Colletotrichum* genomes relied on 72 and 333 sequences, respectively (see **fig. S2** legend and
412 **Table S3** for more details). The phylogenetic analysis of the peroxidase-catalase superfamily
413 relied on 150 sequences encompassing Class I (intracellular peroxidases), II (fungal secreted
414 peroxidases) and III (plant secreted peroxidases) peroxidases and from so-called Hybrid B
415 peroxidases, as previously reported (52). Subsequently to manual curation (removing signal
416 peptides), the sequences were first aligned using MAFFT-DASH (L-INS-i method) (53) and
417 the resulting multiple sequence alignment (MSA) was used to infer a phylogenetic tree using
418 RAxML (1000 bootstraps). The trees were then visualized in iTOL (54) and edited in
419 Illustrator®.

420 For the gene neighborhood survey, we retrieved 4 genes located upstream and downstream of
421 each *Colletotrichum*'s AA5_2 query (72 sequences). The resulting 569 genes were assigned to
422 78 different PFAM domains. The frequency of occurrence of a given type of domain in the
423 neighborhood of each AA5_2 phylogenetic clade was then computed and visualized in Excel.
424 For interrogating the co-occurrence of both Perox and AlcOx-coding genes beyond
425 *Colletotrichum* species two independent BLAST searches were run against the NCBI non-
426 redundant database, using *CorAlcOx* and *CorPerox* as query sequences. 1,000 AlcOx-like
427 (down to 37% sequence identity) and 1,000 Perox-like (25% sequence identity) sequences
428 along with their corresponding source microorganism were retrieved. A cross-comparison of
429 both lists of microorganisms, applying different sequence identity-based thresholds (60% for
430 AlcOx and 30% for Perox) returned the list of species harboring both type of enzymes.

431 Transcriptomics data were retrieved from publicly available datasets (26–29). To normalize
432 different dataset longitudinally, we expressed reported sampling time points as infection stages
433 in Fig. 1 as follows (hpi = hours post-infection): for *C. fructicola nara gc5/strawberry* (27),
434 AP (24 hpi), BP (72 hpi) and NP (144 hpi); for *C. orbiculare/N. benthamiana* (27), AP (24
435 hpi), BP (72 hpi) and NP (168 hpi); for *C. higginsianum/A. thaliana* (26), AP (22 hpi), BP (40
436 hpi) and NP (60 hpi); *C. graminicola/Maize* (26), AP (22 hpi), BP (40 hpi) and NP (60 hpi);

437 *M. oryzae/Rice* (28), AP (8 hpi), BP (24 hpi) and NP (48 hpi); *M. oryzae/Barley* (29), AP (12
438 hpi), PP (24 hpi), BP (36 hpi) and NP (48 hpi).

439

440 **Structure Prediction and Preparation**

441 *Surface hydrophobicity*

442 Structural homology models were generated with AlphaFold (55) and surface hydrophobicity
443 of selected CROs was computed with the “protein-sol patches” online software (56). Average
444 hydrophobicity of the binding surface was determined as follows: using PyMOL 2.4, we
445 selected the residues constituting the entire binding surface of *FgrGalOx*, *CgrAlcOx* and
446 equivalent residues (based on MSA) in orthologous enzymes (5 GalOx and 11 AlcOx in total)
447 as well as those of 4 characterized hydrophobins (PDB 2N4O, 2LSH, 1R2M and 2FZ6) as
448 hydrophobic protein reference. Average hydrophobicity of the selected residues was computed
449 as a GRAVY index score (Kyte-Doolittle method) (57).

450 *Preparation of models for docking experiments*

451 We used Alphafold2 (55) to obtain a model for *CorAlcOx* and *CorPerOx*. To add the metals
452 and cofactors to AlphaFold2 models, we performed a BLAST search in the Protein Data Bank
453 proteins database and selected the PDB 2EIC (Sequence Identity 47%) to add the copper to
454 *CorAlcOx*, and the PDB 1MN2 (Sequence Identity 28%) to add the calcium ions and the heme
455 group to *CorPerox*. Subsequently, we prepared the systems with Schrödinger Protein
456 Preparation Wizard (58) to determine the protonation states at pH 7 using PROPKA (59), and
457 finally relax the systems performing a restrained minimization with convergence criteria for
458 heavy atoms to 0.30 Å using the OPLS_2005 force field.

459 *Protein-Protein Docking*

460 For the generation of protein-protein poses (PPPs), we used PIPER (35) to generate 70,000
461 PPPs, which were clustered with the in-built clustering protocol using the default RMSD
462 threshold of 9.0 Å and a minimum population of 10 poses per cluster. In parallel, we also used
463 the recently developed Alphafold2 Multimer (36), which only uses sequence information,
464 together with ion and cofactor placements, as described above.

465 *PPPs refinement with PELE*

466 We used the all atom Monte Carlo (MC) software PELE (Protein Energy Landscape
467 exploration), to map intermolecular interactions (37, 60). PELE follows a heuristic MC
468 approach, generating new conformational proposals using vibration modes of the proteins with
469 translations and rotations of the ligand (*CorPerox* in this case), and relaxing the system with
470 structure prediction methods, so that the probability of acceptance in the Metropolis criterion
471 (61) remains high (60). Here, we refined the top five PIPER and five AlphaFold2-Multimer
472 models, using a simulation of 250 PELE steps with 256 computing cores (about 25 independent
473 trajectories per model). Each MC PELE step consists of a perturbation and a relaxation stage.
474 In the first one, a perturbation of the ligand, *CorAlcOx* in this case, is first performed, including
475 random rotations of 0.01-0.04 rad and translations of 0.25-0.50 Å, and is followed by a
476 backbone perturbation of both proteins following the normal modes directions predicted by an
477 Anisotropic Network Model (ANM). In the second stage, the system is first relaxed by a high
478 resolution side chain prediction including all protein-protein interphase side chains, defined by

479 the region within 3 Å of any heavy atom of the other protein. Afterwards, a global minimization
480 is performed to relax the entire system, providing a final conformation and energy; this energy
481 is then used in a Metropolis importance sampling to accept/reject the MC step.

482 *Exploring the substrate interactions*

483 The C18 substrate was created with Maestro 3D Builder, followed by a Glide docking (62) on
484 the lowest energy PPPs, as predicted with PELE. The docking grid was defined with a cubic
485 box of 30 Å centered in between the copper ion and Tyr120(OH) of the *CorAlcOx*. Following
486 the Glide rigid receptor docking, we performed a C18 induced fit rescoring simulation
487 involving 40 PELE steps (using 48 computing cores). Each PELE step consisted of a random
488 rotation of 0.01-0.04 rad and translation of 0.05-0.15 Å, using a spherically restrained search
489 space of radius 12 Å centered on the copper ion. The perturbation step was then followed by a
490 relaxation phase including side chain prediction (all side chains inside the spherical space) and
491 a full system minimization.

492 **DNA cloning and strain production**

493 DNA cloning and strain production of the AA5_2 alcohol oxidases (AlcOx) from
494 *Colletotrichum graminearum* (*CgrAlcOx*, Genbank ID XM_008096275.1, Uniprot ID
495 E3QHV8) was already carried out in previous study (19). The intron-free sequences of the
496 genes coding for the AlcOx from *Colletotrichum orbiculare* MAFF 240422 (*CorAlcOx*,
497 Genbank ID TDZ17043.1, Uniprot ID N4UTF2), the AlcOx from *Magnaporthe oryzae*
498 (*MorAlcOx*, Genbank ID XM_003719321.1, Uniprot ID G4NG45), the Tandem Peroxidase
499 (*Perox*) from *Colletotrichum orbiculare* (*CorPerox*, Genbank ID TDZ17044.1, Uniprot ID
500 N4UUY4) and the Tandem Peroxidase from *Magnaporthe oryzae* (*MorPerox*, Genbank ID
501 XM_003719322.1, Uniprot ID G4NG46) were synthesized after codon optimization for
502 expression in *P. pastoris* and inserted into a modified pPICZaC vector using *XhoI** and *NotI*
503 restriction sites in frame with the α secretion factor at N-terminus (i.e. without native signal
504 peptide) and with a (His)₆-tag at the C-terminus (without *c-myc* epitope) (Genewiz, Leipzig,
505 Germany). Transformation of competent *P. pastoris* X33, selection of zeocin-resistant
506 *P. pastoris* transformants screened for protein production was carried out as described by Haon
507 et al. (63). The best-producing transformants were conserved as glycerol stock at – 80°C.

508 **Heterologous protein production in flasks**

509 All proteins were first produced in 2 L Erlenmeyer flasks. To this end, single colonies of *P.*
510 *pastoris* X33 expressing each gene of interest were individually streaked on a YPD agar plate
511 containing Zeocin (100 µg.mL⁻¹) and incubated 3 days at 30°C. A single colony was then used
512 to inoculate 5 mL of YPD, in a 50 mL sterile Falcon tube and incubated during 5 h (30°C, 160
513 rpm). This pre-culture was used to inoculate at 0.2% (vol/vol) 500 mL of BMGY medium, in
514 a 2 L Erlenmeyer flask, incubated during approximately 16 h (30°C, 200 rpm) until the OD₆₀₀
515 nm reached 4–6. The produced cellular biomass was then harvested by centrifugation (5 min,
516 16°C, 3,000 x g). For the AlcOx, the cell pellet was then resuspended in 100 mL BMMY
517 medium supplemented with methanol (1%, vol/vol) and CuSO₄ (500 µM). The culture was
518 incubated for 3 days (16°C, 200 rpm), with daily additions of methanol (1% added, vol/vol).
519 The Tandem Peroxidases production conditions were optimized and varied from the standard
520

522 protocol as follows: the BMMY was supplemented with methanol (3% vol/vol), hemin (25
523 μM) and CaCl_2 (2 mM). The culture was incubated for 3 days (20°C, 200 rpm), with daily
524 additions of methanol (3%, vol/vol) and hemin (25 μM). Then, the extracellular medium was
525 recovered by centrifugation (10 min, 4°C, 3,000 x g) and the supernatant filtrated on 0.45 μm
526 membrane (Millipore, Massachusetts, USA) and stored at 4°C prior to purification.

527

528 **Heterologous protein production in bioreactors**

529 The upscaled production of *CorPerox* was carried out in 1.3 L and 7.5 L bioreactors (New
530 Brunswick BioFlo 115 fermentor, Eppendorf, Germany) as per the *P. pastoris* fermentation
531 process guidelines (Invitrogen) with the following optimizations: the glycerol fed-batch phase
532 was replaced by a sorbitol and methanol transition phase, besides 200 μM (1.3 L bioreactor)
533 and 150 μM (7.5 L bioreactor) of hemin were added to the methanol solution. CaCl_2 (10 mM
534 final) was added to the crude protein solution before being either directly purified or flash-
535 frozen in liquid nitrogen and stored at -80°C. We verified that flash-freezing did not cause any
536 activity loss, for both AlcOx and Perox enzymes.

537

538 **Protein purification**

539 The filtered *CorAlcOx* and *MorAlcOx* crude supernatants were adjusted to pH 8.5, filtered on
540 0.22 μm filters (Millipore, Molsheim, France), and purified by anion exchange
541 chromatography (DEAE) on a HiPrep FF 16/10 column (GE Healthcare, USA). Elution was
542 performed by applying a linear gradient from 0 to 500 mM NaCl (in Tris-HCl buffer 50 mM,
543 pH 8.5) over 20 column volumes, with a flow rate set to 5 mL.min⁻¹.

544 The filtered *CorPerox* and *MorPerox* culture supernatant was adjusted to pH 7.8 just before
545 purification and filtered on 0.22 μm filters (Millipore, Molsheim, France). Depending on the
546 volume to purify, the crude protein sample was either loaded on a His-Trap HP 5-mL column
547 (GE Healthcare, Buc, France) on a HiPrep FF 16/10 column (GE Healthcare) connected to an
548 ÄKTExpress system (GE Healthcare) equilibrated with HEPES (10 mM, pH 8.0), NaCl (100
549 mM), CaCl_2 (2 mM) and imidazole (10 mM) buffer. Each (His)₆-tagged recombinant enzyme
550 was eluted with HEPES (10 mM, pH 8.0), NaCl (100 mM), CaCl_2 (2 mM) and imidazole (500
551 mM) buffer. The Tandem Peroxidases were further purified by size exclusion chromatography,
552 using a HiLoad 26/600 Superdex 200 pg column (GE Healthcare) operated at 2.5 mL/min and
553 with a running buffer containing HEPES (10 mM, pH 8.0), NaCl (100 mM) and CaCl_2 (2 mM).
554 After SDS-PAGE analysis, fractions containing the recombinant enzyme were pooled,
555 concentrated and buffer exchanged in sodium phosphate (50 mM, pH 7.0) for the AlcOx or in
556 HEPES (10 mM, pH 8.0), NaCl (100 mM) and CaCl_2 (2 mM) buffer for the Tandem
557 Peroxidases.

558 Protein concentrations of *CgrAlcOx* (52,337 Da, $\epsilon^{280} = 101,215 \text{ M}^{-1}.\text{cm}^{-1}$), *CorAlcOx* (52,317
559 Da, $\epsilon^{280} = 92,735 \text{ M}^{-1}.\text{cm}^{-1}$), *MorAlcOx* (62,894 Da, $\epsilon^{280} = 90,020 \text{ M}^{-1}.\text{cm}^{-1}$), *CorPerox* (26,137
560 Da, $\epsilon^{280} = 21,345 \text{ M}^{-1}.\text{cm}^{-1}$), and *MorPerox* (26,290 Da, $\epsilon^{280} = 24,450 \text{ M}^{-1}.\text{cm}^{-1}$) were
561 determined by the Bradford assay (64) using BSA as reference protein as well as by UV
562 absorption at 280 nm using a Nanodrop ND-200 spectrophotometer (Thermo Fisher Scientific,
563 Massachusetts, USA).

564

565

566

567 **Enzyme assays**

568 For screening the substrate specificity of CRO-AlcOx enzymes, the alcohol substrates were
569 prepared in sodium phosphate buffer (50 mM, pH 7.0) in 96-well microplates and reactions
570 were initiated by the addition of a pre-mix of CRO-AlcOx (1 nM final concentration), HRP
571 (0.1 mg.mL⁻¹) and 2,2'-azino-bis(3-ethylbenzothiazoline-6-sulfonic acid (ABTS, 500 μM) in
572 sodium phosphate buffer (50 mM, pH 7.0). The tested substrates included D-glucose (50 mM
573 final concentration, D-Glc), D-galactose (50 mM, D-Gal), D-raffinose (50 mM, D-Raf),
574 xyloglucan (0.1% mM, XG), butan-1-ol (3 mM), butan-2-ol (3 mM), octan-1-ol (3 mM),
575 decan-1-ol (3 mM), 2,4-hexadiene-1-ol (3 mM, HD-OH), glycol aldehyde dimer (3 mM,
576 GAD), benzyl alcohol (3 mM, BnOH), 4-hydroxybenzyl alcohol (3 mM, p-OH BnOH), vanillic
577 alcohol (3 mM, Van-OH), syringic alcohol (3 mM, Syr-OH) and cinnamyl alcohol (3 mM, Cin-
578 OH). The absorbance of the final reaction (100 μL total volume) was monitored at 414 nm
579 using a microplate spectrophotometer (TECAN), thermostated at 23°C. The 414 nm
580 absorbance allows to determine the concentration of ABTS cation radical over time (ABTS^{•+},
581 $\epsilon^{414} = 31,100 \text{ M}^{-1} \cdot \text{cm}^{-1}$), and in turn the rate of alcohol oxidation, considering a peroxidase
582 reaction stoichiometry for (H₂O₂:ABTS^{•+}) of 1:2 and a CRO-AlcOx reaction stoichiometry for
583 (alcohol:H₂O₂) of 1:1.

584 For screening the substrate specificity of *CorPerox*, unless stated otherwise the enzyme (0.125
585 μM final) was prepared in citrate-phosphate buffer (50 mM, pH 4.0 to 7.0) in 96-well
586 microplates (for wavelength in the visible range) or in 1 mL Quartz cuvettes (for UV range),
587 in the presence of various substrates (*vide infra*). Reactions were initiated by the addition of
588 H₂O₂ (100 μM final), incubated at 23°C, and monitored spectrophotometrically at the
589 wavelengths indicated below. The tested peroxidase substrates included: ABTS (500 μM)
590 converted into ABTS^{•+} ($\epsilon^{414} = 31,100 \text{ M}^{-1} \cdot \text{cm}^{-1}$); 2,6-dimethoxyphenol (2,6-DMP, 500 μM)
591 converted into hydrocoerulignone ($\epsilon^{469} = 53,200 \text{ M}^{-1} \cdot \text{cm}^{-1}$); guaiacol (500 μM) converted into
592 the final product tetraguaiacol ($\epsilon^{470} = 26,600 \text{ M}^{-1} \cdot \text{cm}^{-1}$); Reactive Black 5 (RB5, 100 μM, ϵ^{600}
593 $= 20,000 \text{ M}^{-1} \cdot \text{cm}^{-1}$) converted into non-chromogenic product RB5^{ox}; veratryl alcohol (500 μM)
594 converted into veratraldehyde ($\epsilon^{310} = 9,300 \text{ M}^{-1} \cdot \text{cm}^{-1}$). For testing the manganese peroxidase
595 activity, *CorPerox* was mixed with Mn(II)SO₄ (1 mM final) in tartrate buffer (50 mM, pH 2.0
596 to 5.0) and the formation of Mn³⁺-tartrate complex upon addition of H₂O₂ (100 μM) was
597 followed at 238 nm ($\epsilon^{238} = 6,500 \text{ M}^{-1} \cdot \text{cm}^{-1}$), as previously described (65).

598 All activities were expressed as Vi/E (s⁻¹), i.e. the initial rate (Vi, μmoles of H₂O₂ consumed
599 per second) divided by the amount of enzyme (in μmoles).

600 *CorPerox* stability over time was carried out by monitoring the peroxidase activity of *CorPerox*
601 samples (50 μM) stored in sodium acetate buffer (50 mM, pH 5.2), at 4°C, in the presence of
602 varying concentrations of CaCl₂ (0-500 mM). The peroxidase activity of these samples was
603 measured as described above (final concentration of 0.5 μM *CorPerox*), using ABTS (500 μM)
604 and H₂O₂ (100 μM) as substrates, in citrate-phosphate buffer (50 mM, pH 4.0), at 23°C.

605 Michaelis-Menten kinetic parameters of *CorPerox* were determined by measuring the
606 peroxidase initial rate, as described above, in the presence of ABTS (500 μM) and varying

607 concentrations of H₂O₂ (0-1200 μM), in citrate-phosphate buffer (50 mM, pH 4.0), at 23°C.
608 Experimental data could be fit to the standard Michaelis-Menten equation (residual standard
609 error = 0.019).

610 AlcOx activation by the peroxidases was assayed by monitoring changes in absorbance at 254
611 nm upon oxidation of benzyl alcohol (1.5 mM) into benzaldehyde by the CRO (10 nM final
612 concentration), in the presence of varying concentrations of peroxidase (0-1000 nM). Reactions
613 were carried out in sodium-phosphate buffer (50 mM, pH 7.0), at 23°C, in UV-transparent
614 cuvettes (1 mL reaction volume). The reactions were initiated by addition of the CRO and
615 vigorously mixed by pipetting up and down. The absorbance was measured using an Evolution
616 201 UV-Vis spectrophotometer (Thermo-Fisher). The concentration of benzaldehyde was
617 calculated as $[\text{Benzaldehyde}]_t = (\text{Abs}^{254 \text{ nm}}_t - \text{Abs}^{254 \text{ nm}}_{t0}) / (\epsilon^{254}_{\text{benzaldehyde}} - \epsilon^{254}_{\text{BnOH}})$, where
618 $\epsilon^{254}_{\text{benzaldehyde}} = 8,500 \text{ M}^{-1} \cdot \text{cm}^{-1}$ and $\epsilon^{254}_{\text{BnOH}} = 150 \text{ M}^{-1} \cdot \text{cm}^{-1}$.

619

620 **Gas chromatography (GC) analysis**

621 Enzymatic reactions were carried out in 4 mL-clear borosilicate glass vials closed by screw
622 caps with PTFE septum (500 μL final reaction volume). *CorAlcOx* (2 μM final) was mixed
623 with *CorPerox* (2 μM) in sodium phosphate buffer (50 mM, pH 7.0). The reaction was initiated
624 by the addition of octadecanol (0.3 mg.mL⁻¹, eq. 1.1 mM final) and the mixture was incubated
625 at 23°C at 190 rpm in an Innova 42R incubator (New Brunswick, USA), during 1 h. Following
626 a previously published protocol (22), the reaction mixture was then acidified by addition of 10
627 μL HCl (12 M). Products and possible remaining substrate were extracted by adding 500 μL
628 of hexane (containing 1 mM of internal standard dodecane), followed by shaking and
629 centrifugation for 5 min at 3,000 x g. The organic layer was transferred into a new vial and
630 analyzed with a GC-2010 Plus apparatus (Shimadzu, Japan) equipped with a flame ionization
631 detector (FID) and a DB-5 capillary column (30 m x 0.25 mm x 0.25 μm; Agilent). Nitrogen
632 (200 kPa) was used as carrier gas. The injector and detector temperatures were set at 250°C.
633 After injection (2 μL sample), the analytes were separated by applying the following
634 temperature program: step 1) from 65°C to 250°C over 9.25 min (i.e. 20°C/min); step 2) plateau
635 at 250°C for 6 min. For quantitation, standard curves of octadecanol, *n*-octadecanal and
636 octadecanoic acid were prepared by following the same procedure.

637

638 **Electron Paramagnetic Resonance (EPR)**

639 EPR spectra were recorded on frozen solutions (120K) using a Bruker Elexsys E500
640 spectrometer operating at X-band equipped with a BVT 3000 digital temperature controller.
641 The following acquisition parameters were used: modulation frequency 100 kHz; modulation
642 amplitude 5 G; gain 87 dB; and microwave power, 20 mW. EPR spectra were simulated using
643 the EasySpin toolbox developed for Matlab (66). *CorAlcOx* (100 μM final), prepared in
644 sodium phosphate buffer (50 mM, pH 7.0), in the absence or presence of *CorPerox* (100 μM
645 final), was flash-frozen in liquid nitrogen and continuous-wave EPR spectra were recorded.
646 *CorAlcOx* and *CorPerox* were placed in contact for various amount of time (2.5 min, 15 min)
647 before flash-freezing the solution. Controls containing buffer only or the *CorPerox* were also
648 carried out.

649

650 **Analysis of cuticular waxes from cucumber cotyledons**

651 Cuticular waxes were extracted from 2-weeks old cotyledons by immersing 6 intact cotyledons
652 for 30 s in chloroform in a glass beaker. Chloroform was evaporated under a stream of nitrogen
653 gas and wax extracts were derivatized using N,O-Bis (trimethylsilyl)trifluoroacetamide
654 (BSTFA) and analyzed by gas chromatography coupled to mass spectrometry (GC-MS) as
655 previously described (67).

656
657 **Strains and media**

658 Strain 104-T (MAFF240422) of *C. orbiculare* was used as the wild-type strain. All strains used
659 in this study are listed in **Table S4** (13, 38, 68–70). *C. orbiculare* strains were cultured on 3.9%
660 PDA (Nissui) at 24°C in darkness. For genetic manipulation, *Escherichia coli* DH5 α -
661 competent cells were maintained on Luria-Bertani (LB) agar at 37°C. For fungal
662 transformation, *Agrobacterium tumefaciens* C58C1 was maintained on LB agar at 28°C.
663 Transformations of *C. orbiculare* (13, 38) were carried out as previously described.

664
665 **Strain construction**

666 Primers and plasmids used in this study are listed in **Table S5**. For construction of *CorAlcOx*
667 deletion strains, 1.1-kb upstream and 1.0-kb downstream flanking sequences and a 1.0-kb
668 fragment of the neomycin-resistance cassette was amplified with the respective primer pairs.
669 For construction of *CorPerox* deletion strains, 1.1-kb upstream and downstream flanking
670 sequences and a 1.4-kb fragment of the hygromycin-resistance cassette was amplified. These
671 three fragments were inserted into linearized pPZP-PvuII using the In-Fusion HD cloning kit
672 (Clontech). The same procedures were used for construction of *M. oryzae* gene deletion strains.
673 For construction of *CorAlcOx-mCherry* and *CorPerox-GFP* gene fusion, a 5.9-kb *CorAlcOx*-
674 *CorPerox* fragment containing 1.1-kb downstream flanking sequences was inserted into
675 linearized pPZP-PvuII-SUR, and the mCherry and GFP fragments were inserted.
676 For construction of *CorAlcOx-mCherry* overexpression strains, a 4.0-kb *CorAlcOx-mCherry*
677 fragment containing its 1.1-kb downstream flanking sequence was amplified from pPZP-
678 *AlcOx-mCherry-Perox-GFP-S*, and fused to linearized pCAMSUR-TEF (71) containing the
679 translation elongation factor promoter of *Aureobasidium pullulans* (72). The same procedures
680 were used for construction of *CorPerox-GFP* overexpression strains.

681
682 **Plant infection**

683 Infection assays on detached cucumber leaves (*Cucumis sativus* L. ‘Suyo’) with conidial
684 suspension (1×10^5 conidia/ml in distilled water) of *C. orbiculare* were performed as previously
685 described (73). The inoculated leaves were incubated in a humid environment for 5 days at
686 24°C. For testing the effect of *n*-octadecanal supplementation, conidial suspensions (1×10^5
687 conidia/mL in 10 μ M *n*-octadecanal dissolved in 1% ethanol or 1% ethanol as a control) were
688 spotted onto detached cucumber leaves, and incubated in a humid environment for 5 days at
689 24°C.

690
691 **Microscopy**

692 For observation of appressorium formation of *C. orbiculare*, a conidial suspension (5×10^5
693 conidia/ml) was placed on a multiwell glass slide or cover glass (Matsunami Glass),

694 respectively. Cells were incubated in a humid box for 24 h at 24°C in the dark. Observation of
695 penetration hyphae on cucumber cotyledons and cellophane membranes were performed as
696 previously described (13). Appressorial cytorrhysis assay was conducted based on a previous
697 procedure (68).

698 A confocal laser scanning microscope LSM900 with Airyscan 2 (Carl Zeiss) equipped with a
699 Plan Apochromat 63×/1.4 Oil DIC objective (Carl Zeiss) was used to acquire confocal
700 microscopic images. Excitation/emission wavelengths were 488 nm/490-556 nm for GFP and
701 561 nm/565-630 nm for mCherry. Images were acquired and processed using ZEN Software
702 (Version 3.1; Carl Zeiss) and Imaris (Version 9.3.1; Bitplane). For detection of appressorial
703 actin assembly, cells were observed using a Zeiss Axio Imager M2 Upright microscope (Carl
704 Zeiss) equipped with a Plan Apochromat 100× oil immersion lens, an Axio Cam MRm digital
705 camera and excitation/barrier filter set of 595 nm/620 nm for RFP. Images were acquired using
706 Axiovision 4.8. Bright-field microscopy was performed using a Nikon ECLIPSE E600
707 microscope equipped with a 40× water immersion lens (Nikon) and an OLYMPUS DP74
708 digital camera system.

709

710

711 **Microarray analysis**

712 For sampling appressoria, the abaxial surface of cucumber cotyledons or cellophane
713 membranes (Wako Chemicals) were inoculated with 10 µL droplets or 10 mL, respectively, of
714 a conidial suspension (1×10^6 conidia/ml), and then incubated at 24°C in a humid box. After
715 16 h, the cellophane was frozen in liquid nitrogen. After 24 h, the lower epidermis of the
716 cotyledons was peeled off. All samples were ground in liquid nitrogen, and total RNA was
717 prepared using the Maxwell RSC Plant RNA Kit (Promega) and the Agilent Plant RNA
718 Isolation MiniKit (Agilent Technologies). Microarray analyses were performed as described
719 previously (13) using the *C. orbiculare* ($8 \times 60,000$, 13,352 independent probes, Design ID:
720 060762) oligo microarray, according to the Agilent 60-mer Oligo Microarray Processing
721 Protocol (Agilent Technologies). The normalization condition: i) intensity-dependent Lowess
722 normalization; ii) data transformation, measurements less than 0.01 were set to 0.01; iii) per-
723 chip 75th-percentile normalization of each array; and iv) the expression values per gene were
724 median normalized. The normalized data were subjected to a *t* test, with statistically significant
725 gene sets defined as those giving *P* values less than 0.05. The differentially-regulated genes
726 (fold change > 2 and *P* < 0.05) were selected and were used for further analysis. Functional
727 classification was based on the Gene Ontology (GO), protein families (Pfam) and *C. orbiculare*
728 genome information of CAZymes and SSPs. Note that to avoid redundancy in the count of up-
729 and downregulated genes, all sequences considered as CAZymes were not counted in the
730 broader classes of Hydrolases/Transferases/Oxidoreductases.

731 **References and Notes:**

- 732 1. S. Kamoun, N. J. Talbot, M. Tofazzal Islam, Plant health emergencies demand open science: Tackling a
733 cereal killer on the run. *PLoS Biol.* **17**, 1–6 (2019).
- 734 2. M. C. Fisher, N. J. Hawkins, D. Sanglard, S. J. Gurr, Worldwide emergence of resistance to antifungal
735 drugs challenges human health and food security. *Science.* **360**, 739–742 (2018).
- 736 3. R. Dean, J. A. L. Van Kan, Z. A. Pretorius, K. E. Hammond-Kosack, A. Di Pietro, P. D. Spanu, J. J. Rudd,
737 M. Dickman, R. Kahmann, J. Ellis, G. D. Foster, The Top 10 fungal pathogens in molecular plant
738 pathology. *Mol. Plant Pathol.* **13**, 414–430 (2012).
- 739 4. C. Beimforde, K. Feldberg, S. Nylinder, J. Rikkinen, H. Tuovila, H. Dörfelt, M. Gube, D. J. Jackson, J.
740 Reitner, L. J. Seyfullah, A. R. Schmidt, Estimating the Phanerozoic history of the Ascomycota lineages:
741 Combining fossil and molecular data. *Mol. Phylogenet. Evol.* **78**, 386–398 (2014).
- 742 5. X. Liang, B. Wang, Q. Dong, L. Li, J. A. Rollins, R. Zhang, G. Sun, Pathogenic adaptations of
743 *Colletotrichum* fungi revealed by genome wide gene family evolutionary analyses. *PLoS One.* **13**,
744 e0196303 (2018).
- 745 6. L. S. Ryder, N. J. Talbot, Regulation of appressorium development in pathogenic fungi. *Curr. Opin. Plant*
746 *Biol.* **26**, 8–13 (2015).
- 747 7. J. C. De Jong, B. J. McCormack, N. Smirnoff, N. J. Talbot, Glycerol generates turgor in rice blast. *Nature.*
748 **389**, 244–245 (1997).
- 749 8. Y. Kubo, I. Furusawa, in *The Fungal Spore and Disease Initiation in Plants and Animals*, G. T. Cole, H.
750 C. Hoch, Eds. (Springer US, Boston, MA, 1991), pp. 205–218.
- 751 9. Z. Chen, M. C. Silva, C. J. Rodriguesjr, Appressorium Turgor Pressure of *Colletotrichum kahawae* Might
752 Have a Role in Coffee Cuticle Penetration. *Mycologia.* **96**, 1199–1208 (2004).
- 753 10. L. S. Ryder, Y. F. Dagdas, M. J. Kershaw, C. Venkataraman, A. Madzvamuse, X. Yan, N. Cruz-Mireles,
754 D. M. Soanes, M. Osés-Ruiz, V. Styles, J. Sklenar, F. L. H. Menke, N. J. Talbot, A sensor kinase controls
755 turgor-driven plant infection by the rice blast fungus. *Nature.* **574**, 423–427 (2019).
- 756 11. M. He, J. Su, Y. Xu, J. Chen, M. Chern, M. Lei, T. Qi, Z. Wang, L. S. Ryder, B. Tang, M. Osés-Ruiz, K.
757 Zhu, Y. Cao, X. Yan, I. Eisermann, Y. Luo, W. Li, J. Wang, J. Yin, S. M. Lam, G. Peng, X. Sun, X. Zhu,
758 B. Ma, J. Wang, J. Liu, H. Qing, L. Song, L. Wang, Q. Hou, P. Qin, Y. Li, J. Fan, D. Li, Y. Wang, X.
759 Wang, L. Jiang, G. Shui, Y. Xia, G. Gong, F. Huang, W. Wang, X. Wu, P. Li, L. Zhu, S. Li, N. J. Talbot,
760 X. Chen, Discovery of broad-spectrum fungicides that block septin-dependent infection processes of
761 pathogenic fungi. *Nat. Microbiol.* **5**, 1565–1575 (2020).
- 762 12. Y. F. Dagdas, K. Yoshino, G. Dagdas, L. S. Ryder, E. Bielska, G. Steinberg, N. J. Talbot, Septin-mediated
763 plant cell invasion by the rice blast fungus, *Magnaporthe oryzae*. *Science.* **336**, 1590–1595 (2012).
- 764 13. S. Kodama, J. Ishizuka, I. Miyashita, T. Ishii, T. Nishiuchi, H. Miyoshi, Y. Kubo, The morphogenesis-
765 related NDR kinase pathway of *Colletotrichum orbiculare* is required for translating plant surface signals
766 into infection-related morphogenesis and pathogenesis. *PLOS Pathog.* **13**, e1006189 (2017).
- 767 14. R. O. Rocha, C. Elowsky, N. T. T. Pham, R. A. Wilson, Spermium-mediated tight sealing of the
768 *Magnaporthe oryzae* appressorial pore–rice leaf surface interface. *Nat. Microbiol.* **5**, 1472–1480 (2020).
- 769 15. M. C. Giraldo, B. Valent, Filamentous plant pathogen effectors in action. *Nat. Rev. Microbiol.* **11**, 800–
770 814 (2013).
- 771 16. A. Djamei, K. Schipper, F. Rabe, A. Ghosh, V. Vincon, J. Kahnt, S. Osorio, T. Tohge, A. R. Fernie, I.
772 Feussner, K. Feussner, P. Meinicke, Y.-D. Stierhof, H. Schwarz, B. Macek, M. Mann, R. Kahmann,
773 Metabolic priming by a secreted fungal effector. *Nature.* **478**, 395–398 (2011).
- 774 17. J. A. D. Cooper, W. Smith, M. Bacila, H. Medina, Galactose Oxidase from *Polyporus circinatus*, Fr.*. *J.*
775 *Biol. Chem.* **234**, 445–448 (1959).
- 776 18. P. J. Kersten, T. K. Kirk, Involvement of a new enzyme, glyoxal oxidase, in extracellular H₂O₂ production
777 by *Phanerochaete chrysosporium*. *J. Bacteriol.* **169**, 2195–2201 (1987).
- 778 19. D. (Tyler) Yin, S. Urresti, M. Lafond, E. M. Johnston, F. Derikvand, L. Ciano, J.-G. Berrin, B. Henrissat,
779 P. H. Walton, G. J. Davies, H. Brumer, Structure–function characterization reveals new catalytic diversity
780 in the galactose oxidase and glyoxal oxidase family. *Nat. Commun.* **6**, 10197 (2015).
- 781 20. Y. Mathieu, W. A. Offen, S. M. Forget, L. Ciano, A. H. Viborg, E. Blagova, B. Henrissat, P. H. Walton,
782 G. J. Davies, H. Brumer, Discovery of a Fungal Copper Radical Oxidase with High Catalytic Efficiency
783 toward 5-Hydroxymethylfurfural and Benzyl Alcohols for Bioprocessing. *ACS Catal.* **10**, 3042–3058
784 (2020).
- 785 21. S. B. Lee, M. C. Suh, Advances in the understanding of cuticular waxes in *Arabidopsis thaliana* and crop
786 species. *Plant Cell Rep.* **34**, 557–572 (2015).
- 787 22. D. Ribeaucourt, B. Bissaro, M. Yemloul, V. Guallar, H. Brumer, F. Lambert, J.-G. Berrin, M. Lafond,
788 Controlled Oxidation of Long-Chain Primary Aliphatic Alcohols by a Fungal Copper-Radical Alcohol
789 Oxidase. *ACS Sustain. Chem. Eng.* **9**, 4411–4421 (2021).

- 790 23. K. Parikka, M. Tenkanen, Oxidation of methyl α -D-galactopyranoside by galactose oxidase: products
791 formed and optimization of reaction conditions for production of aldehyde. *Carbohydr. Res.* **344**, 14–20
792 (2009).
- 793 24. S. M. Forget, F. R. Xia, J. E. Hein, H. Brumer, Determination of biocatalytic parameters of a copper
794 radical oxidase using real-Time reaction progress monitoring. *Org. Biomol. Chem.* **18**, 2076–2084 (2020).
- 795 25. A. Zerva, P. Christakopoulos, E. Topakas, Characterization and application of a novel class II
796 thermophilic peroxidase from *Myceliophthora thermophila* in biosynthesis of polycatechol. *Enzyme
797 Microb. Technol.* **75–76**, 49–56 (2015).
- 798 26. R. J. O’Connell, M. R. Thon, S. Hacquard, S. G. Amyotte, J. Kleemann, M. F. Torres, U. Damm, E. A.
799 Buiate, L. Epstein, N. Alkan, J. Altmüller, L. Alvarado-Balderrama, C. A. Bauser, C. Becker, B. W.
800 Birren, Z. Chen, J. Choi, J. A. Crouch, J. P. Duvick, M. A. Farman, P. Gan, D. Heiman, B. Henrissat, R.
801 J. Howard, M. Kabbage, C. Koch, B. Kracher, Y. Kubo, A. D. Law, M. H. Lebrun, Y. H. Lee, I. Miyara,
802 N. Moore, U. Neumann, K. Nordström, D. G. Panaccione, R. Panstruga, M. Place, R. H. Proctor, D.
803 Prusky, G. Rech, R. Reinhardt, J. A. Rollins, S. Rounsley, C. L. Schardl, D. C. Schwartz, N. Shenoy, K.
804 Shirasu, U. R. Sikhakolli, K. Stüber, S. A. Sukno, J. A. Sweigard, Y. Takano, H. Takahara, F. Trail, H.
805 C. Van Der Does, L. M. Voll, I. Will, S. Young, Q. Zeng, J. Zhang, S. Zhou, M. B. Dickman, P. Schulze-
806 Lefert, E. Ver Loren Van Themaat, L. J. Ma, L. J. Vaillancourt, Lifestyle transitions in plant pathogenic
807 *Colletotrichum* fungi deciphered by genome and transcriptome analyses. *Nat. Genet.* **44**, 1060–1065
808 (2012).
- 809 27. P. Gan, K. Ikeda, H. Irieda, M. Narusaka, R. J. O’Connell, Y. Narusaka, Y. Takano, Y. Kubo, K. Shirasu,
810 Comparative genomic and transcriptomic analyses reveal the hemibiotrophic stage shift of *Colletotrichum*
811 fungi. *New Phytol.* **197**, 1236–1249 (2013).
- 812 28. Y. Dong, Y. Li, M. Zhao, M. Jing, X. Liu, M. Liu, X. Guo, X. Zhang, Y. Chen, Y. Liu, Y. Liu, W. Ye, H.
813 Zhang, Y. Wang, X. Zheng, P. Wang, Z. Zhang, Global Genome and Transcriptome Analyses of
814 *Magnaporthe oryzae* Epidemic Isolate 98-06 Uncover Novel Effectors and Pathogenicity-Related Genes,
815 Revealing Gene Gain and Lose Dynamics in Genome Evolution. *PLoS Pathog.* **11**, 1–30 (2015).
- 816 29. M. Shimizu, Y. Nakano, A. Hirabuchi, K. Yoshino, M. Kobayashi, K. Yamamoto, R. Terauchi, H. Saitoh,
817 RNA-Seq of in planta-expressed *Magnaporthe oryzae* genes identifies MoSVP as a highly expressed gene
818 required for pathogenicity at the initial stage of infection. *Mol. Plant Pathol.* **20**, 1682–1695 (2019).
- 819 30. Y. Kubo, Y. Takano, Dynamics of infection-related morphogenesis and pathogenesis in *Colletotrichum*
820 *orbiculare*. *J. Gen. Plant Pathol.* **79**, 233–242 (2013).
- 821 31. J. N. Rodriguez-Lopez, A. T. Smith, R. N. F. Thorneley, Role of Arginine 38 in Horseradish Peroxidase.
822 A critical residue for substrate binding and catalysis. *J. Biol. Chem.* **271**, 4023–4030 (1996).
- 823 32. B. Bissaro, A. Varnai, Å. K. Røhr, V. G. H. Eijsink, Oxidoreductases and reactive oxygen species in
824 lignocellulose biomass conversion. *Microbiol. Mol. Biol. Rev.* **82** (2018).
- 825 33. I. Ayuso-Fernández, F. J. Ruiz-Dueñas, A. T. Martínez, Evolutionary convergence in lignin-degrading
826 enzymes. *Proc. Natl. Acad. Sci. U. S. A.* **115**, 6428–6433 (2018).
- 827 34. S. Oide, Y. Tanaka, A. Watanabe, M. Inui, Carbohydrate-binding property of a cell wall integrity and
828 stress response component (WSC) domain of an alcohol oxidase from the rice blast pathogen *Pyricularia*
829 *oryzae*. *Enzyme Microb. Technol.* **125**, 13–20 (2019).
- 830 35. D. Kozakov, R. Brenke, S. R. Comeau, S. Vajda, PIPER: An FFT-based protein docking program with
831 pairwise potentials. *Proteins Struct. Funct. Bioinforma.* **65**, 392–406 (2006).
- 832 36. R. Evans, M. O’Neill, A. Pritzel, N. Antropova, A. Senior, T. Green, A. Židek, R. Bates, S. Blackwell, J.
833 Yim, O. Ronneberger, S. Bodenstein, M. Zielinski, A. Bridgland, A. Potapenko, A. Cowie, K.
834 Tunyasuvunakool, R. Jain, E. Clancy, P. Kohli, J. Jumper, D. Hassabis, Protein complex prediction with
835 AlphaFold-Multimer. *bioRxiv*. 10.04.463034 (2021). doi:10.1101/2021.10.04.463034.
- 836 37. K. W. Borrelli, A. Vitalis, R. Alcantara, V. Guallar, PELE: Protein energy landscape exploration. A novel
837 Monte Carlo based technique. *J. Chem. Theory Comput.* **1**, 1304–1311 (2005).
- 838 38. F. Fukada, Y. Kubo, *Colletotrichum orbiculare* Regulates Cell Cycle G1/SProgression via a Two-
839 Component GAP and a GTPase to Establish Plant Infection. *Plant Cell.* **27**, 2530–2544 (2015).
- 840 39. K. K. Pennerman, G. Yin, J. W. Bennett, Eight-carbon volatiles: prominent fungal and plant interaction
841 compounds. *J. Exp. Bot.* **73**, 487–497 (2022).
- 842 40. M. Haddad Momeni, F. Fredslund, B. Bissaro, O. Raji, T. V. Vuong, S. Meier, T. S. Nielsen, V. Lombard,
843 B. Guigliarelli, F. Biaso, M. Haon, S. Grisel, B. Henrissat, D. H. Welner, E. R. Master, J. G. Berrin, M.
844 Abou Hachem, Discovery of fungal oligosaccharide-oxidising flavo-enzymes with previously unknown
845 substrates, redox-activity profiles and interplay with LPMOs. *Nat. Commun.* **12** (2021).
- 846 41. J. M. Sanz-Martín, J. R. Pacheco-Arjona, V. Bello-Rico, W. A. Vargas, M. Monod, J. M. Díaz-Mínguez,
847 M. R. Thon, S. A. Sukno, A highly conserved metalloprotease effector enhances virulence in the maize
848 anthracnose fungus *Colletotrichum graminicola*. *Mol. Plant Pathol.* **17**, 1048–1062 (2016).
- 849 42. B. Leuthner, C. Aichinger, E. Oehmen, E. Koopmann, O. Müller, P. Müller, R. Kahmann, M. Bölker, P.

- 850 H. Schreier, A H₂O₂-producing glyoxal oxidase is required for filamentous growth and pathogenicity in
851 *Ustilago maydis*. *Mol. Genet. Genomics*. **272**, 639–650 (2005).
- 852 43. A. K. Chaplin, M. L. C. Petrus, G. Mangiameli, M. A. Hough, D. A. Svistunenko, P. Nicholls, D.
853 Claessen, E. Vijgenboom, J. A. R. Worrall, GlxA is a new structural member of the radical copper oxidase
854 family and is required for glycan deposition at hyphal tips and morphogenesis of *Streptomyces lividans*.
855 *Biochem. J.* **469**, 433–444 (2015).
- 856 44. T. M. Vandhana, J.-L. Reyre, S. Danguubiyam, J.-G. Berrin, B. Bissaro, J. Madhuprakash, On the
857 expansion of biological functions of Lytic Polysaccharides Monooxygenases. *New Phytol.* **233**, 2380–
858 2396 (2022).
- 859 45. F. Sabbadin, S. Urresti, B. Henrissat, A. O. Avrova, L. R. J. Welsh, P. J. Lindley, M. Csukai, J. N. Squires,
860 P. H. Walton, G. J. Davies, N. C. Bruce, S. C. Whisson, S. J. McQueen-Mason, Secreted pectin
861 monooxygenases drive plant infection by pathogenic oomycetes. *Science*. **373**, 774–779 (2021).
- 862 46. M. Pickl, M. Fuchs, S. M. Glueck, K. Faber, The substrate tolerance of alcohol oxidases. *Appl. Microbiol.*
863 *Biotechnol.* **99**, 6617–6642 (2015).
- 864 47. E. Morin, S. Miyauchi, H. San Clemente, E. C. H. Chen, A. Pelin, I. de la Providencia, S. Ndikumana, D.
865 Beaudet, M. Hainaut, E. Drula, A. Kuo, N. Tang, S. Roy, J. Viala, B. Henrissat, I. V. Grigoriev, N.
866 Corradi, C. Roux, F. M. Martin, Comparative genomics of *Rhizophagus irregularis*, *R. cerebriforme*, *R.*
867 *diaphanus* and *Gigaspora rosea* highlights specific genetic features in Glomeromycotina. *New Phytol.*
868 **222**, 1584–1598 (2019).
- 869 48. A. R. Wattam, D. Abraham, O. Dalay, T. L. Disz, T. Driscoll, J. L. Gabbard, J. J. Gillespie, R. Gough, D.
870 Hix, R. Kenyon, D. Machi, C. Mao, E. K. Nordberg, R. Olson, R. Overbeek, G. D. Pusch, M. Shukla, J.
871 Schulman, R. L. Stevens, D. E. Sullivan, V. Vonstein, A. Warren, R. Will, M. J. C. Wilson, H. S. Yoo,
872 C. Zhang, Y. Zhang, B. W. Sobral, PATRIC, the bacterial bioinformatics database and analysis resource.
873 *Nucleic Acids Res.* **42**, D581–D591 (2014).
- 874 49. K. Katoh, D. M. Standley, MAFFT Multiple Sequence Alignment Software Version 7: Improvements in
875 Performance and Usability. *Mol. Biol. Evol.* **30**, 772–780 (2013).
- 876 50. J. Castresana, Selection of Conserved Blocks from Multiple Alignments for Their Use in Phylogenetic
877 Analysis. *Mol. Biol. Evol.* **17**, 540–552 (2000).
- 878 51. A. Stamatakis, RAxML version 8: a tool for phylogenetic analysis and post-analysis of large phylogenies.
879 *Bioinformatics*. **30**, 1312–1313 (2014).
- 880 52. M. Zámocký, Š. Janeček, C. Obinger, Fungal Hybrid B heme peroxidases – unique fusions of a heme
881 peroxidase domain with a carbohydrate-binding domain. *Sci. Rep.* **7**, 9393 (2017).
- 882 53. K. Katoh, J. Rozewicki, K. D. Yamada, MAFFT online service: Multiple sequence alignment, interactive
883 sequence choice and visualization. *Brief. Bioinform.* **20**, 1160–1166 (2018).
- 884 54. I. Letunic, P. Bork, Interactive Tree of Life (iTOL) v4: Recent updates and new developments. *Nucleic*
885 *Acids Res.* **47**, 256–259 (2019).
- 886 55. J. Jumper, R. Evans, A. Pritzel, T. Green, M. Figurnov, O. Ronneberger, K. Tunyasuvunakool, R. Bates,
887 A. Židek, A. Potapenko, A. Bridgland, C. Meyer, S. A. A. Kohl, A. J. Ballard, A. Cowie, B. Romera-
888 Paredes, S. Nikolov, R. Jain, J. Adler, T. Back, S. Petersen, D. Reiman, E. Clancy, M. Zielinski, M.
889 Steinegger, M. Pacholska, T. Berghammer, S. Bodenstein, D. Silver, O. Vinyals, A. W. Senior, K.
890 Kavukcuoglu, P. Kohli, D. Hassabis, Highly accurate protein structure prediction with AlphaFold. *Nature*.
891 **596**, 583–589 (2021).
- 892 56. M. Hebditch, J. Warwicker, Web-based display of protein surface and pH-dependent properties for
893 assessing the developability of biotherapeutics. *Sci. Rep.* **9**, 1–9 (2019).
- 894 57. J. Kyte, R. F. Doolittle, A simple method for displaying the hydropathic character of a protein. *J. Mol.*
895 *Biol.* **157**, 105–132 (1982).
- 896 58. G. Madhavi Sastry, M. Adzhigirey, T. Day, R. Annabhimoju, W. Sherman, Protein and ligand preparation:
897 Parameters, protocols, and influence on virtual screening enrichments. *J. Comput. Aided. Mol. Des.* **27**,
898 221–234 (2013).
- 899 59. M. H. M. Olsson, C. R. SØndergaard, M. Rostkowski, J. H. Jensen, PROPKA3: Consistent treatment of
900 internal and surface residues in empirical pK_a predictions. *J. Chem. Theory Comput.* **7**, 525–537 (2011).
- 901 60. J. F. Gilibert, D. Lecina, J. Estrada, V. Guallar, Monte Carlo Techniques for Drug Design : The success
902 case of PELE in *Methods and Principles in Medicinal Chemistry* (John Wiley & Sons, Ltd, pp. 87–103
903 (2018).
- 904 61. N. Metropolis, A. W. Rosenbluth, M. N. Rosenbluth, A. H. Teller, E. Teller, Equation of state calculations
905 by fast computing machines. *J. Chem. Phys.* **21**, 1087–1092 (1953).
- 906 62. R. A. Friesner, J. L. Banks, R. B. Murphy, T. A. Halgren, J. J. Klicic, D. T. Mainz, M. P. Repasky, E. H.
907 Knoll, M. Shelley, J. K. Perry, D. E. Shaw, P. Francis, P. S. Shenkin, Glide: A New Approach for Rapid,
908 Accurate Docking and Scoring. 1. Method and Assessment of Docking Accuracy. *J. Med. Chem.* **47**,
909 1739–1749 (2004).

- 910 63. M. Haon, S. Grisel, D. Navarro, A. Gruet, J. G. Berrin, C. Bignon, Recombinant protein production
911 facility for fungal biomass-degrading enzymes using the yeast *Pichia pastoris*. *Front. Microbiol.* **6**, 1–12
912 (2015).
- 913 64. M. M. Bradford, A rapid and sensitive method for the quantitation of microgram quantities of protein
914 utilizing the principle of protein-dye binding. *Anal. Biochem.* **72**, 248–254 (1976).
- 915 65. M. J. Martínez, F. J. Ruiz-Dueñas, F. Guillén, Á. T. Martínez, Purification and catalytic properties of two
916 manganese peroxidase isoenzymes from *Pleurotus eryngii*. *Eur. J. Biochem.* **237**, 424–432 (1996).
- 917 66. S. Stoll, A. Schweiger, EasySpin, a comprehensive software package for spectral simulation and analysis
918 in EPR. *J. Magn. Reson.* **178**, 42–55 (2006).
- 919 67. R. Ménard, G. Verdier, M. Ors, M. Erhardt, F. Beisson, W. H. Shen, Histone H2B monoubiquitination is
920 involved in the regulation of cutin and wax composition in *Arabidopsis thaliana*. *Plant Cell Physiol.* **55**,
921 455–466 (2014).
- 922 68. S. Tanaka, K. Yamada, K. Yabumoto, S. Fujii, A. Huser, G. Tsuji, H. Koga, K. Dohi, M. Mori, T.
923 Shiraiishi, R. O’Connell, Y. Kubo, *Saccharomyces cerevisiae* SSD1 orthologues are essential for host
924 infection by the ascomycete plant pathogens *Colletotrichum lagenarium* and *Magnaporthe grisea*. *Mol.*
925 *Microbiol.* **64**, 1332–1349 (2007).
- 926 69. M. Kimura, K. Izawa, K. Yoneyama, T. Arie, T. Kamakura, A Novel Transformation System for
927 *Pyricularia Oryzae*: Adhesion of Regenerating Fungal Protoplasts to Collagen-Coated Dishes. *Biosci.*
928 *Biotechnol. Biochem.* **59**, 1177–1180 (1995).
- 929 70. N. Ishida, S. Akai, Relation of Temperature to Germination of Conidia and Appressorium Formation in
930 *Colletotrichum lagenarium*. *Mycologia.* **61**, 382–386 (1969).
- 931 71. K. Saitoh, M. Nishimura, Y. Kubo, N. Hayashi, E. Minami, Y. Nishizawa, Construction of a Binary
932 Vector for Knockout and Expression Analysis of Rice Blast Fungus Genes. *Biosci. Biotechnol. Biochem.*
933 **72**, 1380–1383 (2008).
- 934 72. A. J. Vanden Wymelenberg, D. Cullen, R. N. Spear, B. Schoenike, J. H. Andrews, Expression of green
935 fluorescent protein in *Aureobasidium pullulans* and quantification of the fungus on leaf surfaces.
936 *Biotechniques.* **23**, 686–690 (1998).
- 937 73. G. Tsuji, S. Fujii, S. Tsuge, T. Shiraiishi, Y. Kubo, *Mol. Plant. Microbe. Interact.*, **16**, 315–325 (2003).
- 938 74. A. Levasseur, E. Drula, V. Lombard, P. M. Coutinho, B. Henrissat, Expansion of the enzymatic repertoire
939 of the CAZy database to integrate auxiliary redox enzymes. *Biotechnol. Biofuels.* **6**, 41 (2013).
- 940 75. R. Baroncelli, D. B. Amby, A. Zapparata, S. Sarrocco, G. Vannacci, G. Le Floch, R. J. Harrison, E. Holub,
941 S. A. Sukno, S. Sreenivasaprasad, M. R. Thon, Gene family expansions and contractions are associated
942 with host range in plant pathogens of the genus *Colletotrichum*. *BMC Genomics.* **17**, 1–17 (2016).
- 943 76. T. Choinowski, W. Blodig, K. H. Winterhalter, K. Piontek, The crystal structure of lignin peroxidase at
944 1.70 Å resolution reveals a hydroxy group on the C(β) of tryptophan 171: A novel radical site formed
945 during the redox cycle. *J. Mol. Biol.* **286**, 809–827 (1999).
- 946 77. M. Sundaramoorthy, K. Kishi, M. H. Gold, T. L. Poulos, Preliminary Crystallographic Analysis of
947 Manganese Peroxidase from *Phanerochaete chrysosporium*. *J. Mol. Biol.* **238**, 845–848 (1994).
- 948 78. M. Pérez-Boada, F. J. Ruiz-Dueñas, R. Pogni, R. Basosi, T. Choinowski, M. J. Martínez, K. Piontek, A.
949 T. Martínez, Versatile peroxidase oxidation of high redox potential aromatic compounds: Site-directed
950 mutagenesis, spectroscopic and crystallographic investigation of three long-range electron transfer
951 pathways. *J. Mol. Biol.* **354**, 385–402 (2005).
- 952 79. N. Ito, S. E. V Phillips, C. Stevens, Z. B. Ogel, M. J. McPherson, J. N. Keen, K. D. S. Yadav, P. F.
953 Knowles, Novel thioether bond revealed by a 1.7 Å crystal structure of galactose oxidase. *Nature.* **350**,
954 87–90 (1991).
- 955 80. C. L. L. Pham, A. Rey, V. Lo, M. Soulès, Q. Ren, G. Meisl, T. P. J. Knowles, A. H. Kwan, M. Sunde,
956 Self-assembly of MPG1, a hydrophobin protein from the rice blast fungus that forms functional amyloid
957 coatings, occurs by a surface-driven mechanism. *Sci. Rep.* **6**, 25288 (2016).
- 958 81. N. Ishida, S. Akai, Relation of Temperature to Germination of Conidia and Appressorium Formation in
959 *Colletotrichum lagenarium*. *Mycologia.* **61**, 382–386 (1969).
- 960 82. J. Sperschneider, P. N. Dodds, EffectorP 3.0: Prediction of Apoplastic and Cytoplasmic Effectors in Fungi
961 and Oomycetes. *Mol. Plant. Microbe. Interact.* **35**, 146–156 (2022).
- 962 83. G. Vaaje-Kolstad, Z. Forsberg, J. S. Loose, B. Bissaro, V. G. Eijsink, Structural diversity of lytic
963 polysaccharide monooxygenases. *Curr. Opin. Struct. Biol.* **44**, 67–76 (2017).

965 **Acknowledgments:** We thank Drs. Morin and Lebreton (INRAE Nancy, France) for allowing
966 us to use their in-house tool "Genocomp" for species tree construction. We thank Pamela Gan
967 (RIKEN-CSRS, Japan) for sharing transcriptome data. **Funding:** This study was supported by
968 the “Agence Nationale de la Recherche” and by the Natural Sciences and Engineering Research

969 Council of Canada through the ANR-NSERC project “FUNTASTIC” (ANR-17-CE07-0047,
970 STPGP 493781-16). We are grateful to MANE & Fils and the “Association Nationale
971 Recherche Technologie” (ANRT) for funding the Ph.D. fellowship of D.R. (grant no.
972 2017/1169). Work in Japan was supported by the Japan Society for the Promotion of Science
973 Grants-in-Aid for Scientific Research – KAKENHI, Grant Numbers 15H05780 and 20H02989
974 to Y.K., and 20K15529 to S.K. **Author contributions:** B.B., S.K., R.O’C., M.L., Y.K., and
975 J.G.B. conceived the work. J.G.B and Y.K. coordinated the study. B.B., S.K., H.H., D.R.,
976 A.J.S., V.G., R.O’C., M.L., Y.K., and J.G.B. designed the experiments. B.B., S.K., H.H., D.R.,
977 M.H., S.G., F.B., T.N., A.M.D.R., and A.J.S. performed the experiments. B.B., S.K., H.H.,
978 D.R., A.J.S., S.M.F., H.B., V.G., M.N.R., R.O’C., M.L., Y.K., and J.G.B. analyzed the data.
979 B.B., S.K., Y.K., and J.G.B. wrote the original draft with review and editing from M.L., H.B.,
980 and R.O’C. All authors have approved the final version of the paper. **Competing interests:**
981 Authors declare no competing interests; and **Data and materials availability:** All data is
982 available in the main text or the supplementary materials.

983 **Supplementary Materials:**

984 Figures S1-S11

985 Tables S1-S6

986 Movies S1